PASJ: Publ. Astron. Soc. Japan **50**, 427–463 (1998)

Nuclear-to-Disk Rotation Curves of Galaxies in the Hα and [N II] Emission Lines

Yoshiaki SOFUE,[1] Akihiko TOMITA,[2] Yoshinori TUTUI,[1] Mareki HONMA,[1] and Yoichi TAKEDA[1]

[1]*Institute of Astronomy, The University of Tokyo, Mitaka, Tokyo 181-8588*
[2]*Faculty of Education, Wakayama University, Wakayama 640-8510*

(Received 1988 May 7; accepted 1988 August 23)

Abstract

We have obtained optical CCD spectroscopy along the major axes of 22 nearby spiral galaxies of Sb and Sc types in order to analyze their rotation curves. By subtracting the stellar continuum emission, we have obtained position–velocity (PV) diagrams of the Hα and [N II] lines. We point out that the Hα line is often superposed by a broad stellar absorption feature (Balmer wing) in the nuclear regions, and, therefore, the [N II] line is a better tracer of kinematics in the central few hundred parsec regions. By applying the envelope-tracing technique to the Hα and [N II] PV diagrams, we have derived nucleus-to-disk rotation curves of the observed galaxies. The rotation curves rise steeply within the central few hundred parsecs, indicating a rapidly rotating nuclear disk and mass concentration near the nucleus.

Key words: Galaxies: general — Galaxies: kinematics — Galaxies: nuclei — Galaxies: rotation

1. Introduction

Rotation curves have been derived by optical and H I-line observations in order to study the mass distribution in the disk and halo of spiral galaxies (Rubin et al. 1980, 1982; Bosma 1981; Kent 1986, 1987; Mathewson et al. 1992; Mathewson, Ford 1996; Persic, Salucci 1995; Persic et al. 1996) and of the Galaxy (Clemens 1985; Honma, Sofue 1997). Current optical observations for spiral galaxies have been devoted mainly to the study of massive halo and disk regions; therefore, the spectra were often over-exposed in the central regions due to the bright stellar bulge light, not necessarily providing accurate data for the nuclear rotation curve. H I observations are useful for investigating the halo and total mass for its extended distribution, while they are also not necessarily useful for studying the central few kpc region because of its deficiency.

Recently, we have shown that the CO line emission will be useful for deriving nuclear rotation curves, because of the high central concentration of CO gas and the negligible the extinction, as well as for the available high angular resolution (Sofue 1996, 1997; Sofue et al. 1997, 1998). We have found that the CO rotation curves show a steep nuclear rise within the central few hundred pc, indicating a mass concentration around the nucleus. Since the CO gas usually coexists with H II regions, Hα-line spectroscopy will also be useful to derive nuclear rotation curves, if the bulge light can be adequately subtracted and extinction is small enough. In fact, Rubin et al. (1997) have obtained extensive Hα spectroscopy for Virgo spirals, and have shown a steep rise of the central rotation curves for many galaxies, indicating a mass concentration.

In order to derive detailed nuclear rotation curves for a greater number of galaxies and to examine whether the steep nuclear rise of rotation is universal in spiral galaxies, we have performed optical spectroscopy of 22 spiral galaxies of Sb and Sc types using a 188-cm reflector.

2. Observations

The observed galaxies are listed in table 1 along with their parameters. The CCD spectroscopic observations were made using the Cassegrain spectrometer equipped on the 188-cm reflector at the Okayama Astrophysical Observatory. The observations were carried out on 1997 February 28–March 6, and October 2–8. The original slit length was 5′, and was put across the nuclei; also, the slit position angles were set along the major axes of the galaxies. The Photometrics CCD chip had 512×512 pixels. The spatial resolution was $0\farcs75$ pixel^{-1}, and we binned every 2 pixels in order to increase the signal-to-noise ratio ($1\farcs5$ bin^{-1}). The spectral dispersion was 0.767 Å(velocity spacing of 34.9 km s^{-1}) per pixel. The slit width in the wavelength direction was 0.30 mm in order to obtain the best combination of effective spectral resolution, and signal-to-noise ratio. Considering the slit width, the effective spectral resolution was 1.92 Å, which corresponds to a velocity resolution of 87.1 km s^{-1}. This velocity resolution enabled us to determine the radial

Table 1. Parameters of observed galaxies.

Name	RA(1950) (h m s)	Dec(1950) (° ′ ″)	$V_{\rm helio}$ (km s^{-1})	Size ($'\times'$)	PA (°)	i (°)	$B_T^{0,i}$ (mag)	D (Mpc)	$D_{\rm TF}$ (Mpc)	Type
NGC 1003....	02 36 06.12	+40 39 28.0	627	5.5 × 1.9	97	67	11.54	10.7	11.6	SA(s)cd
NGC 1417....	03 39 28.20	−04 51 50.0	4068	2.7 × 1.7	175	50	12.26	54.1	52.1	SAB(rs)b
UGC 3691....	07 05 10.50	+15 15 33.0	2203	2.2 × 1.1	65	65	12.30	30.0	20.9	SAcd
NGC 2403....	07 32 05.50	+65 42 40.0	131	21.9 × 12.3	127	62	8.46	4.2	3.5	SAB(s)cd
NGC 2590....	08 22 28.50	−00 25 42.0	4998	2.2 × 0.7	77	71	12.99	64.5	70.0	SA(s)bc
NGC 2708....	08 53 36.90	−03 10 05.0	2008	2.6 × 1.3	20	68	12.55	24.6	55.0	SAB(s)b; p?
NGC 2841....	09 18 35.85	+51 11 24.1	638	8.1 × 3.5	147	64	9.81	12.0	23.4	SA(r)b
NGC 2903....	09 29 20.30	+21 43 23.9	556	12.6 × 6.0	17	66	9.13	6.3	8.7	SAB(rs)bc
NGC 3198....	10 16 51.94	+45 48 06.0	663	8.5 × 3.3	35	71	10.55	10.8	11.5	SB(rs)c
NGC 3495....	10 58 40.90	+03 53 43.0	1136	4.9 × 1.2	20	85	11.80	12.8	19.8	Sd
NGC 3521....	11 03 15.48	+00 14 10.7	685	11.0 × 5.1	163	61	9.40	7.2	13.5	SAB(rs)bc;L
NGC 3672....	11 22 30.40	−09 31 12.0	1862	4.2 × 1.9	8	67	11.10	28.4	22.7	SA(s)c
NGC 4062....	12 01 30.50	+32 10 26.0	769	4.1 × 1.7	100	68	11.66	9.7	18.8	SA(s)c
NGC 4321....	12 20 22.89	+16 05 57.7	1571	7.4 × 6.3	30	37	10.00	16.8	14.7	SAB(s)bc;H II
NGC 4448....	12 25 46.10	+28 53 50.0	669	3.9 × 1.4	94	71	11.50	9.7	24.4	SB(r)ab
NGC 4527....	12 31 35.17	+02 55 43.5	1750	6.2 × 2.1	66	69	10.30	22	13.9	Sb(c)
NGC 4565....	12 33 52.00	+26 15 47.0	1227	15.9 × 1.9	136	90	9.59	9.7	14.3	SA(s)b;sp
NGC 4569....	12 34 18.48	+13 26 16.4	−235	9.5 × 4.4	23	69	9.86	16.8	10.3	SAB(rs)ab;L;Sy
NGC 4605....	12 37 47.50	+61 53 00.0	143	5.8 × 2.2	125	69	10.61	4.0	6.0	SB(s)cp
NGC 5033....	13 11 09.23	+36 51 30.6	875	10.7 × 5.0	170	64	10.33	18.7	18.6	SA(s)c
NGC 5907....	15 14 35.90	+56 30 45.4	667	12.8 × 1.4	155	90	10.31	14.9	18.0	SA(s)c;sp
NGC 7331....	22 34 46.66	+34 09 20.9	821	10.5 × 3.7	171	68	9.67	14.3	16.9	SA(s)b;L

Note: L = LINER; Sy = Seyfert; Distance D is estimated by $D = V_{\rm gc}/H_0$, where $V_{\rm gc}$ is the galacto-centric recession velocity and H_0 = 75 km s^{-1}Mpc^{-1}; Distance $D_{\rm TF}$ was estimated by using a Tully–Fisher relation from Pierce and Tully (1992). $B_T^{0,i}$ is the absolute B magnitude corrected for the inclination and extinction. All other parameters were taken from NASA Extragalactic Data Base (NED).

velocity at an error of about 9 km s^{-1} ($\sim$ 0.1 times the resolution), if the signal-to-noise ratio is sufficiently high (e.g., $>$ 5 rms noise).

The exposure time was 1000 s per one spectrum, and we took three spectra for each galaxy, and finally combined them into one spectrum. Therefore, the total exposure time for the final one frame was 3000 s. We subtracted the stellar bulge continuum emission by applying two methods: (1) a background-filtering technique (Sofue, Reich 1979), and (2) a median-average subtraction in the wavelength direction. In the second method, we first obtained the median value in the λ (wavelength) direction at each position (pixel) on the slit (distance along the major axis). The median value in the λ direction gives an averaged value of the CCD counts of the stellar continuum emission, because the λ pixel number including line emissions is much less than that from the continuum part. Both methods (1) and (2) gave almost the same results, while the latter was found to be better when the emission lines are wide and strong, particularly in the central regions. Threfore, we adopt the results from the median-average subtraction method. We then subtracted the atmospheric lines, which showed no variation in intensity and wavelength along the slit.

3. Results

3.1. *Position–Velocity Diagrams*

The upper two panels of figure 1 show the obtained position–velocity diagrams in the Hα and [N II] lines in a contour form, where the abscissa is the relative position in seconds of arc along the major axis. The velocity is heliocentric, referring to the Hα 6562.8 Å and [N II] 6583.4 Å lines. The contours are drawn in logarithm of base 2, with the lowest contour level set at 3 counts. That is, the contours correspond to intensity levels of 3, 6, 12, 24, 48, ... detector counts, respectively.

The vertically drawn dotted line indicates the position of the galaxy center, which is defined as being the intensity-peak in the light of the bulge-continuum. We obtained a continuum-intensity distribution, i.e., intensity (counts) as a function of the position (arcsec), at each wavelength. We thus determined the spatial position corresponding to the continuum-peak at this wavelength. Repeating this procedure at all wavelengths eventually yielded an ensemble of data, all of which may be

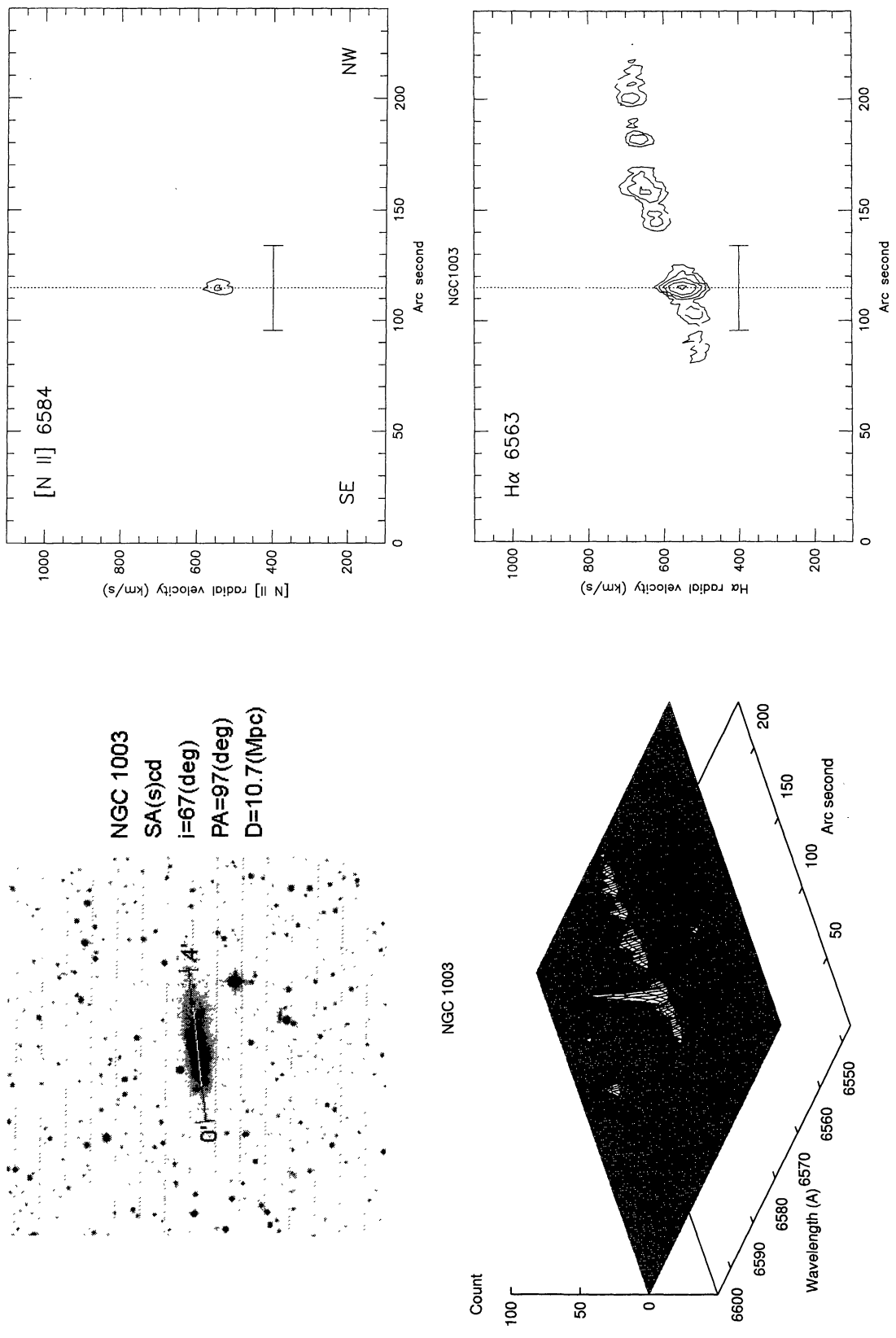

Fig. 1. [Left-upper panels]: 10′ × 10′ image around the center of each galaxy taken from the Digitized-Sky-Survey. The slit position is indicated with the origin (0′) and end (4′) of the slit, corresponding to those of the abscissa in the other panels. [Left-lower panels]: Intensity profiles of the Hα and [N II] lines in the form of 3D plot. The abscissa is the relative displacement along the major axis in arcseconds, and the ordinate the intensity in CCD counts. [Right-upper and lower panels]: [N II]- and Hα-line position–velocity diagrams in contour plots, respectively. The contours are drawn in logarithm of a base 2, with the lowest contour level at 3 CCD counts, which is approximately 3 times the rms noise. The vertical-dashed line indicates the center position of each galaxy, which is the position of maximum intensity in the continuum emission. The horizontal line at the center indicates 2 kpc length (±1 kpc) along the major axis, according to the distance given in table 1.

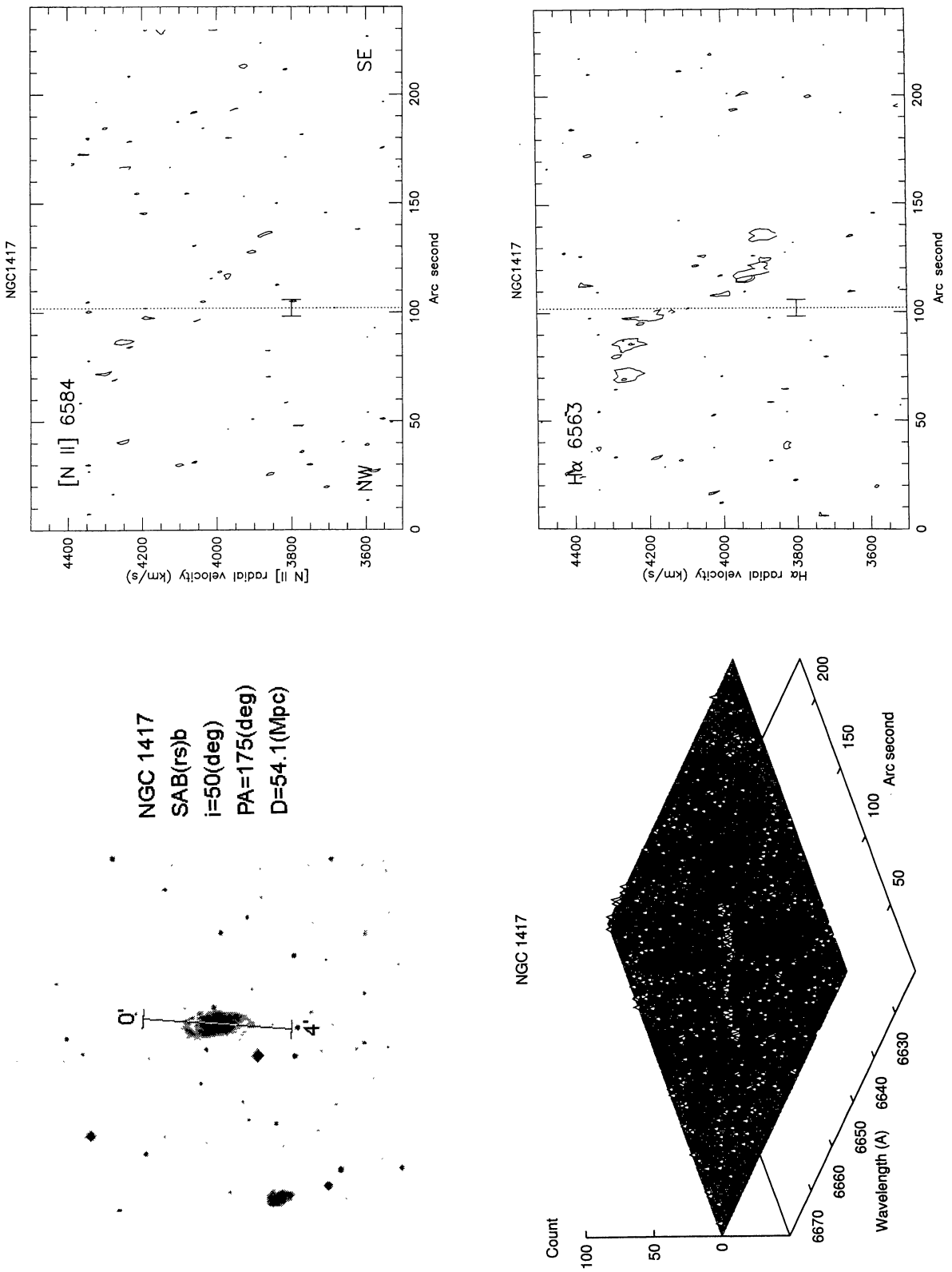

Fig. 1. Continued.

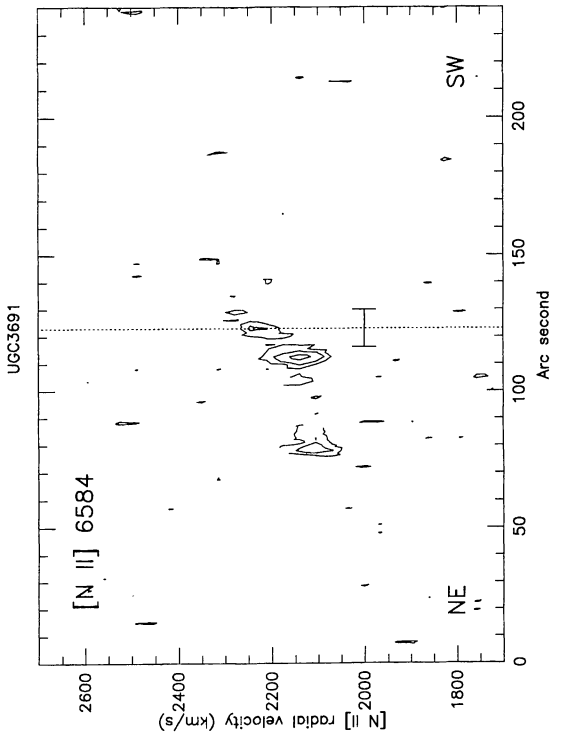

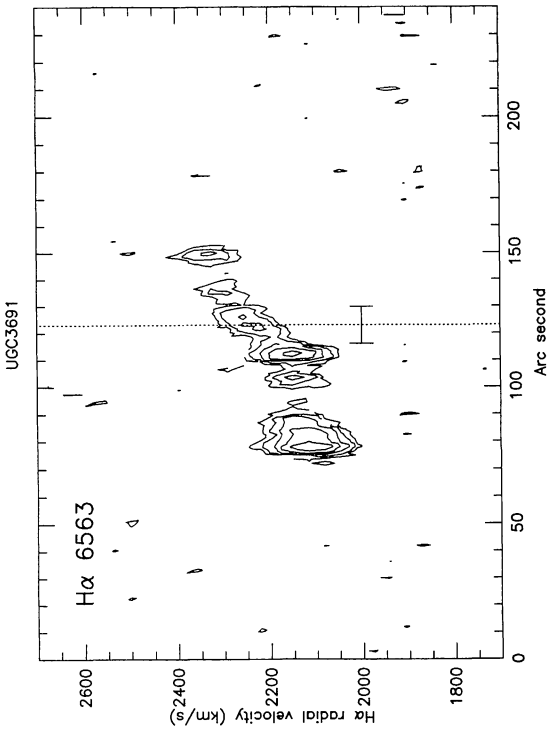

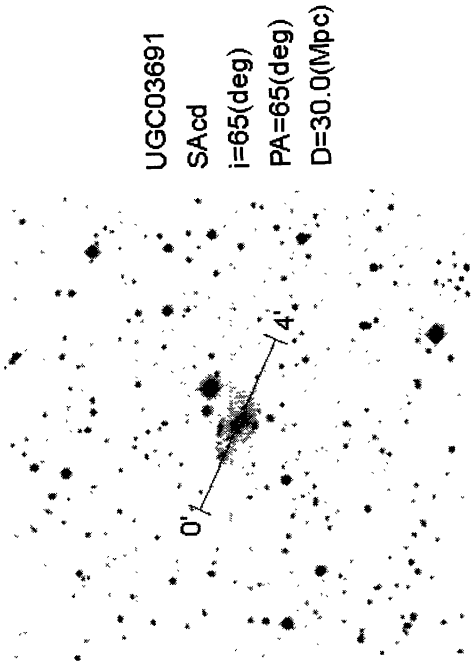

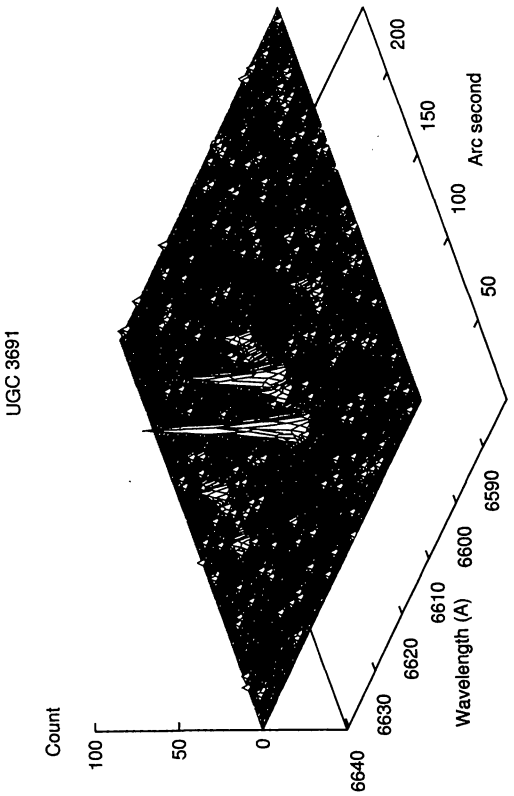

Fig. 1. Continued.

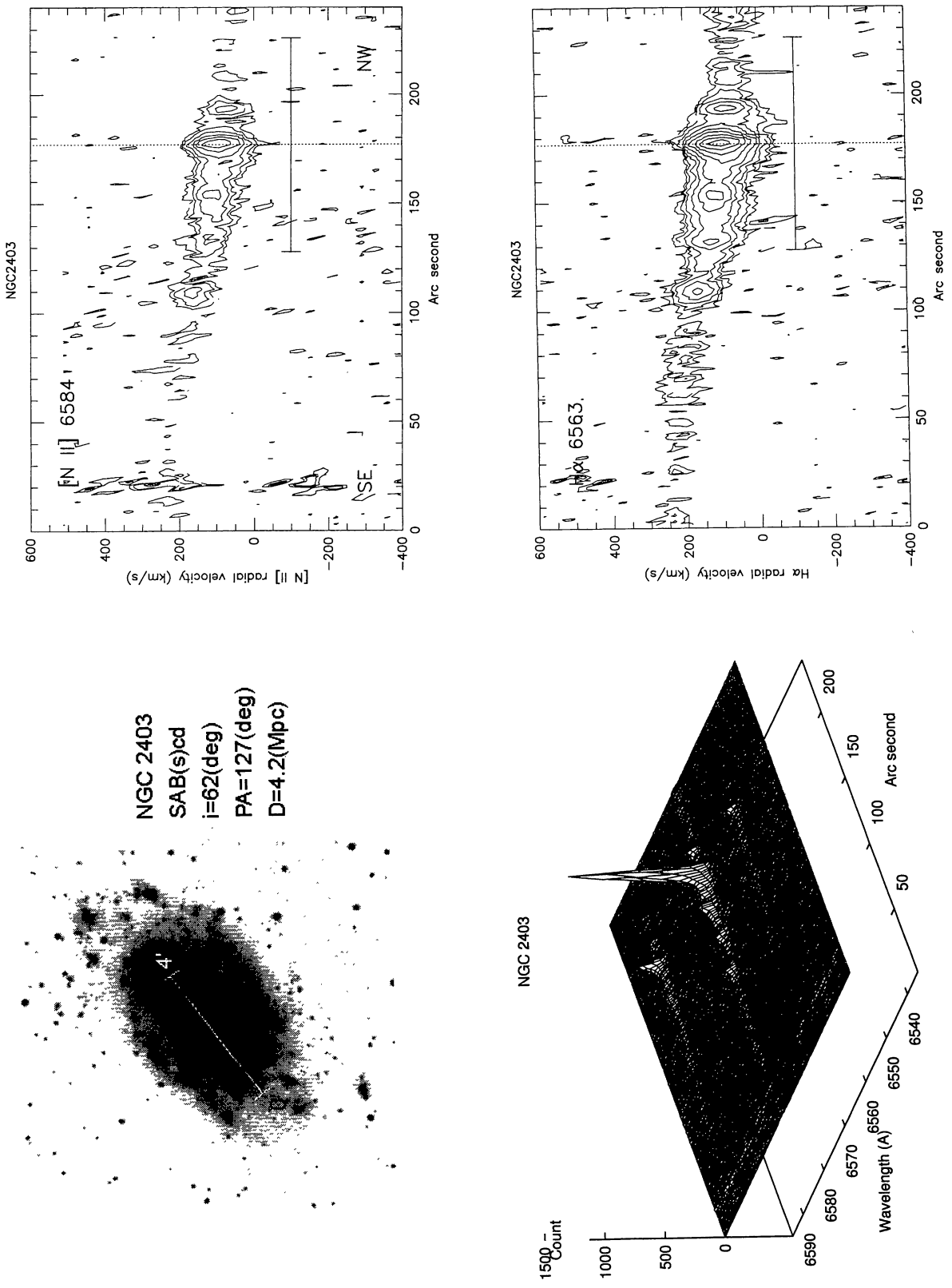

Fig. 1. Continued.

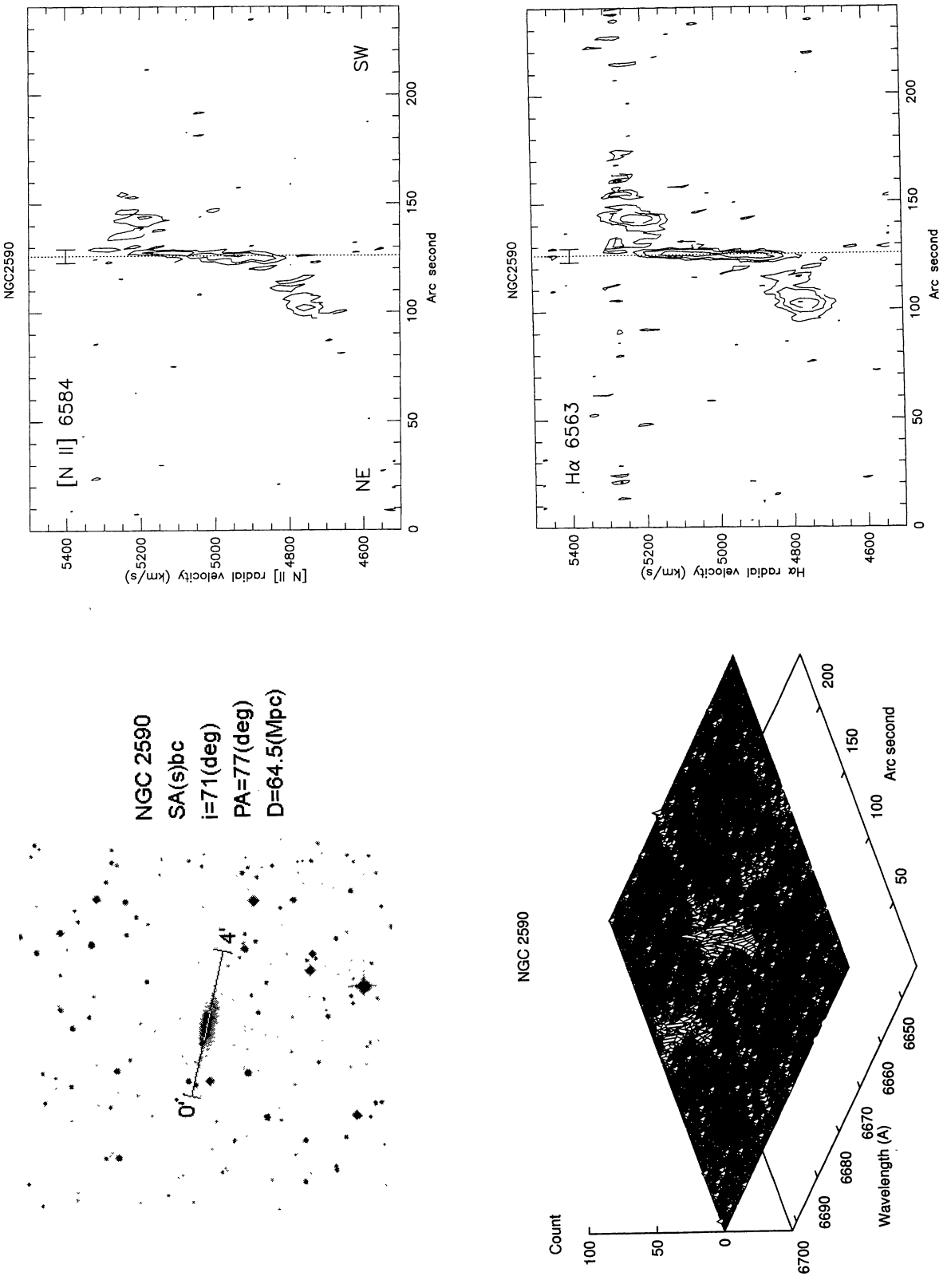

Fig. 1. Continued.

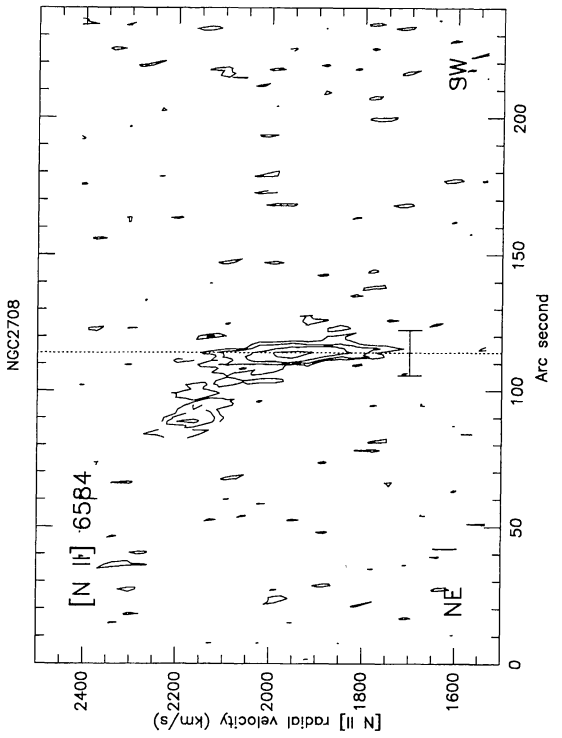

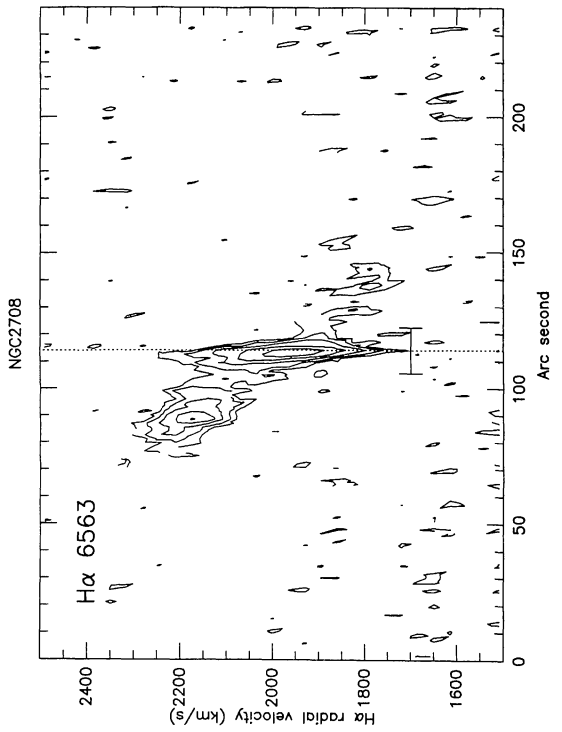

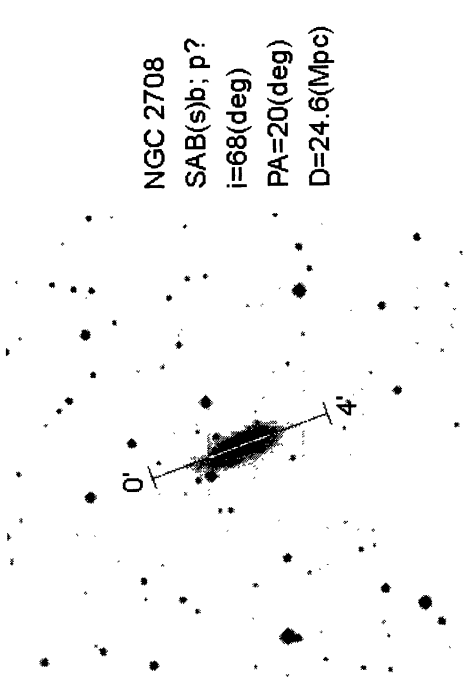

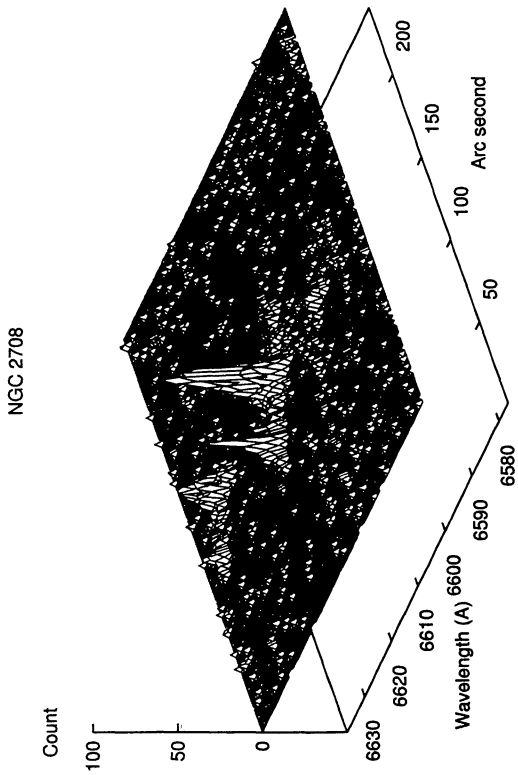

Fig. 1. Continued.

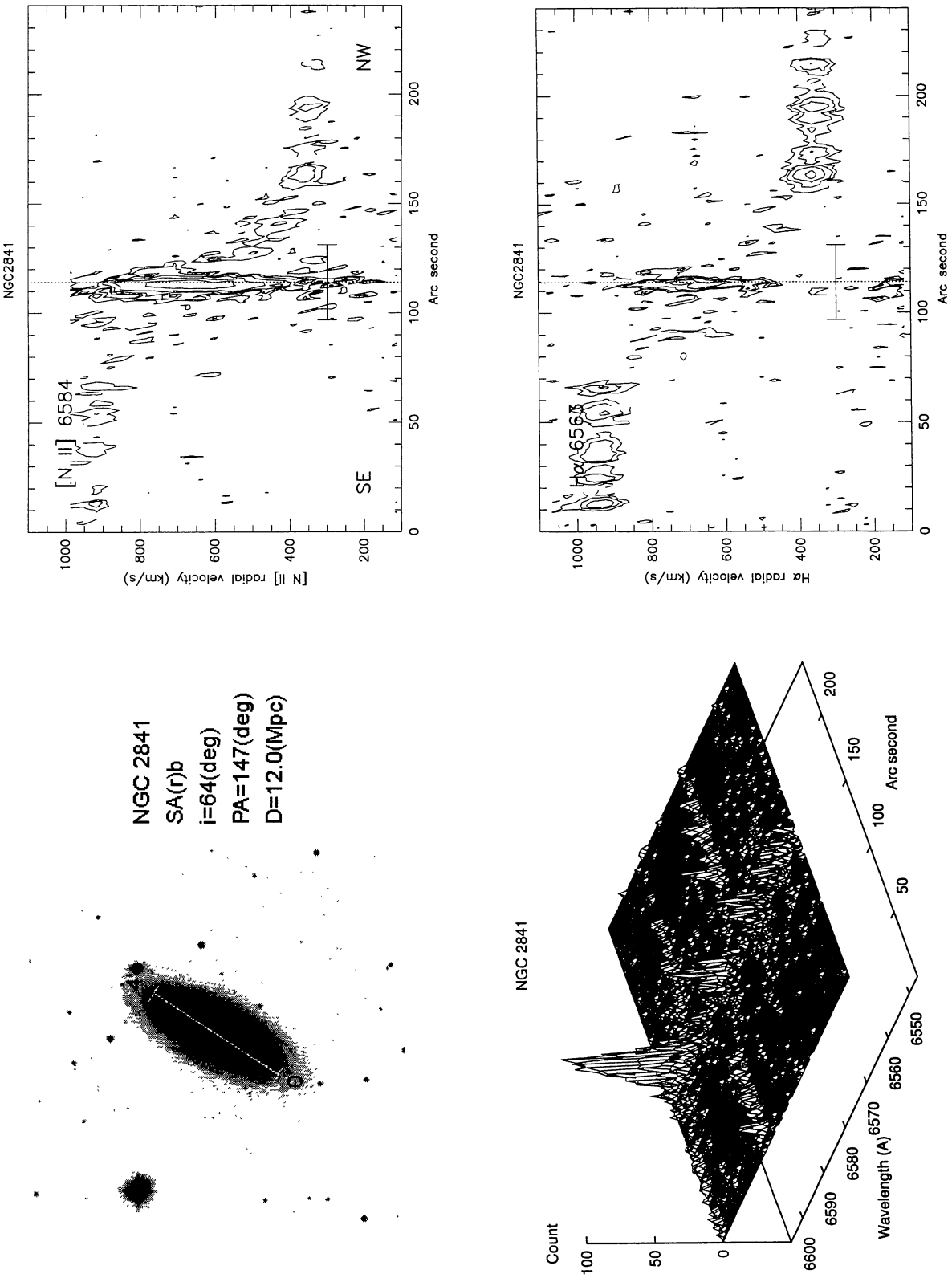

Fig. 1. Continued.

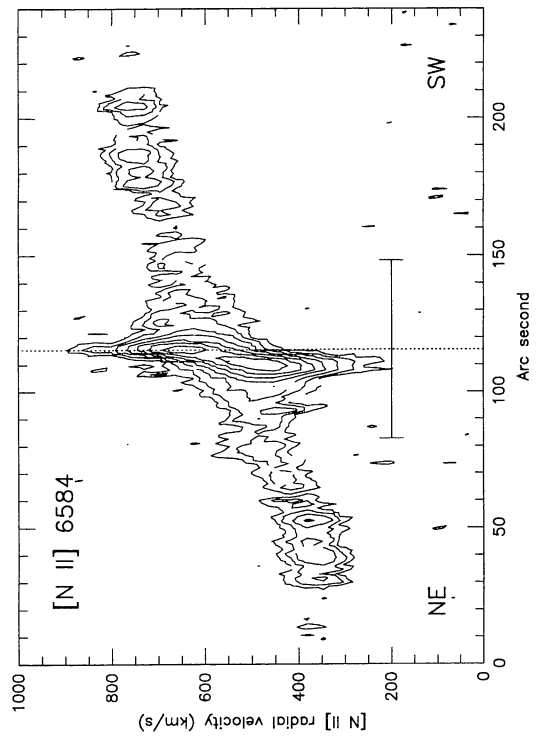

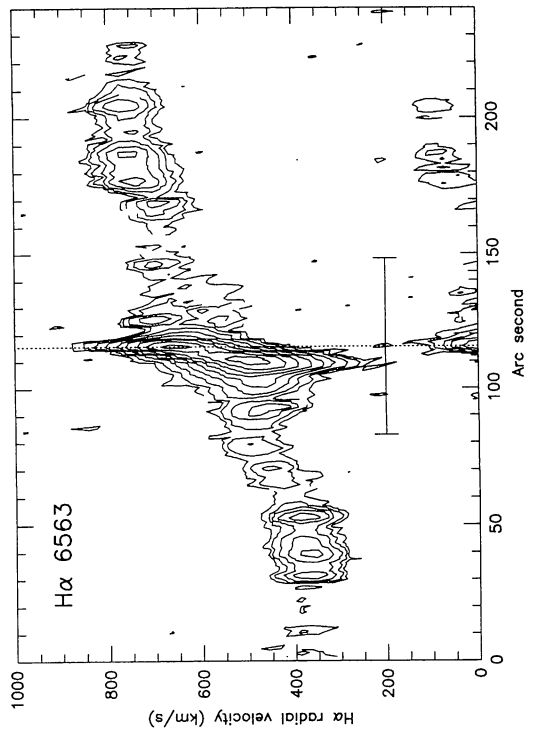

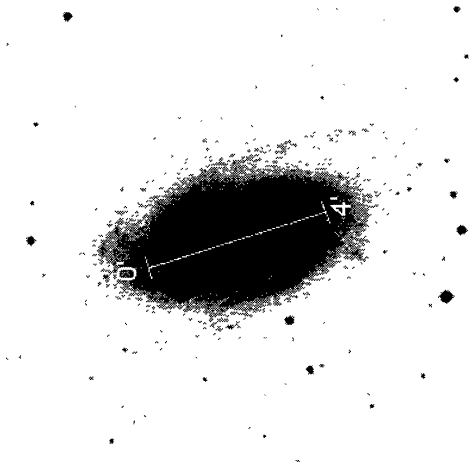

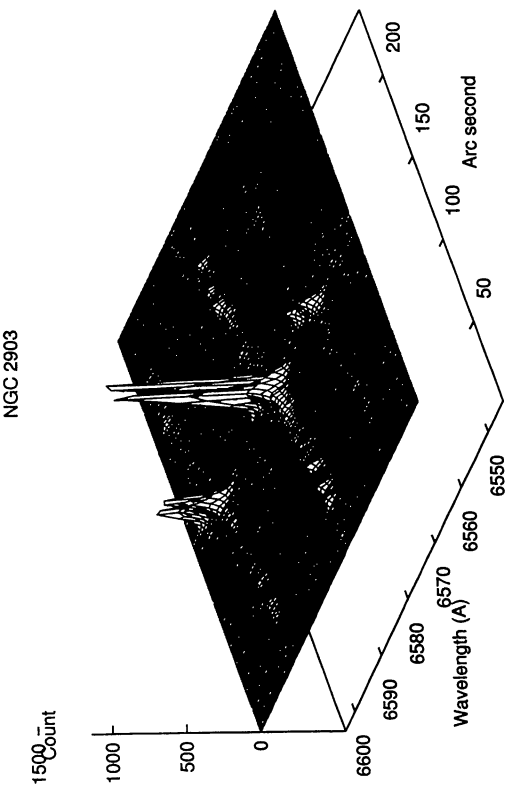

Fig. 1. Continued.

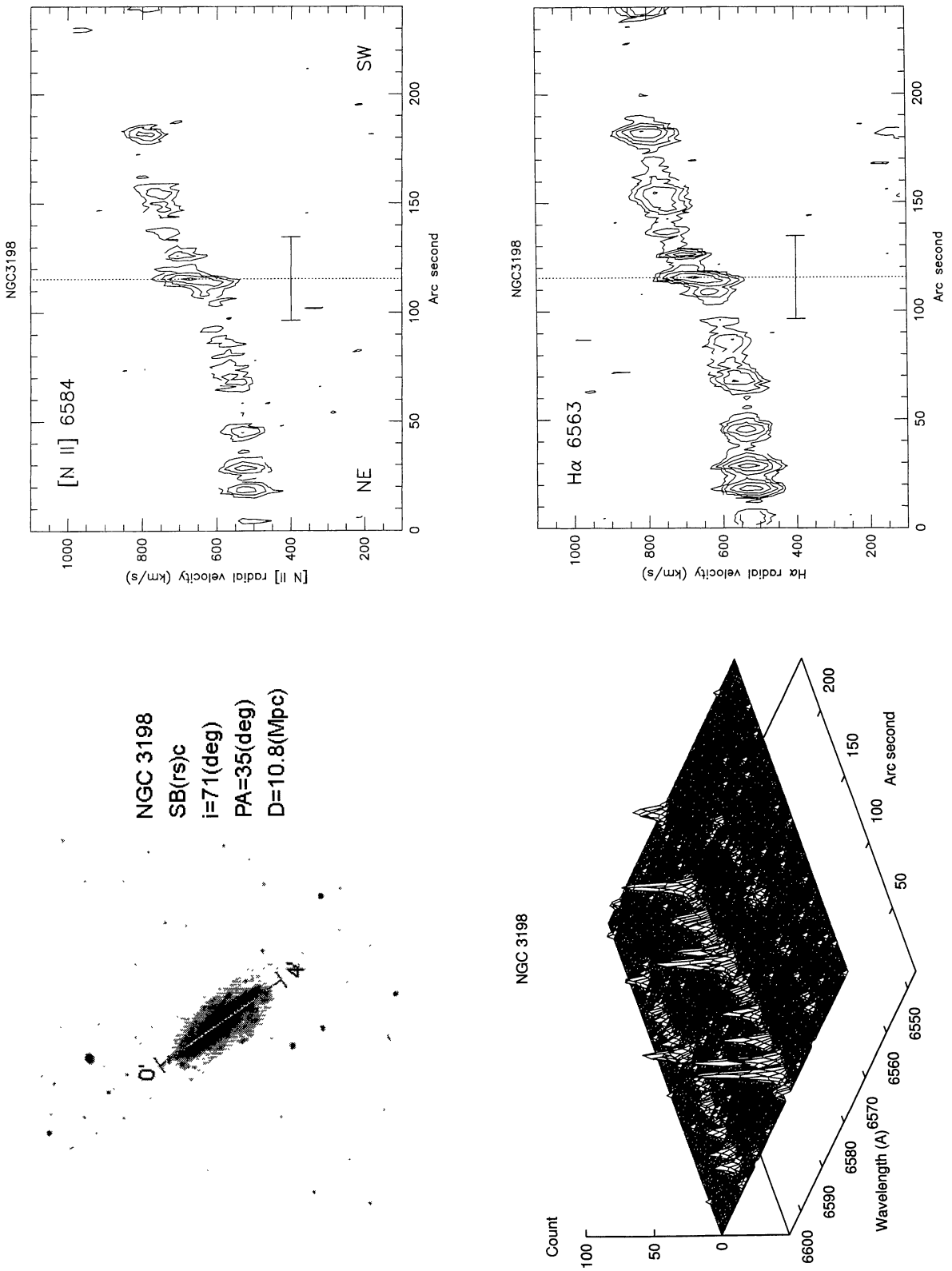

Fig. 1. Continued.

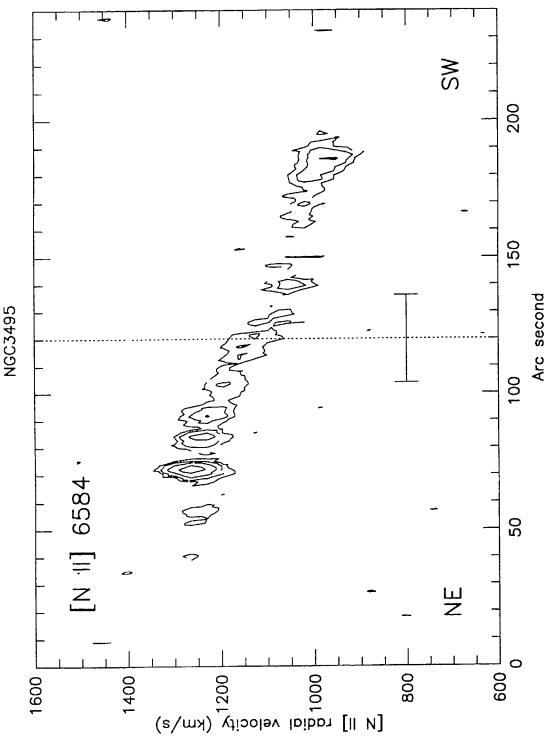

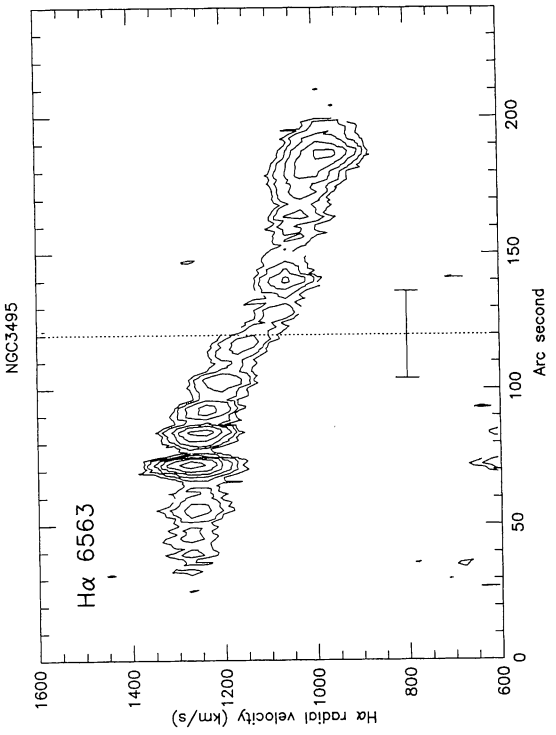

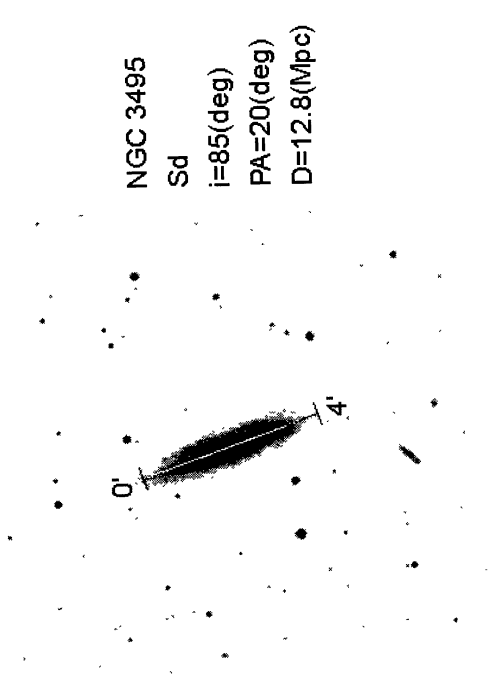

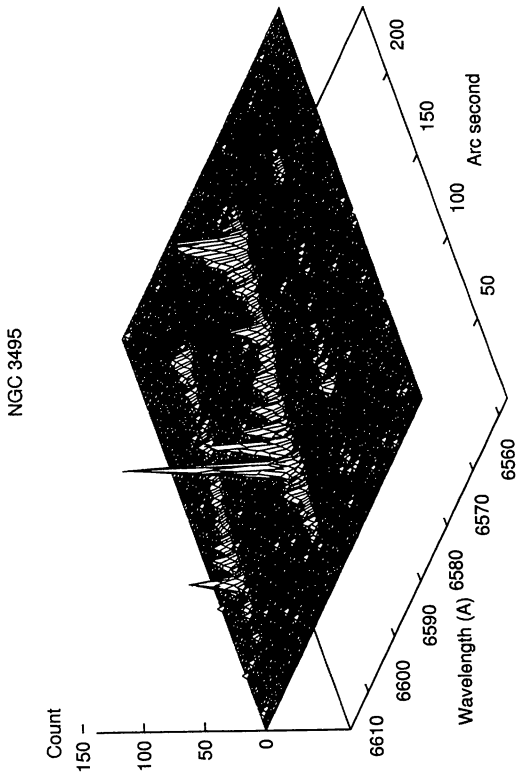

Fig. 1. Continued.

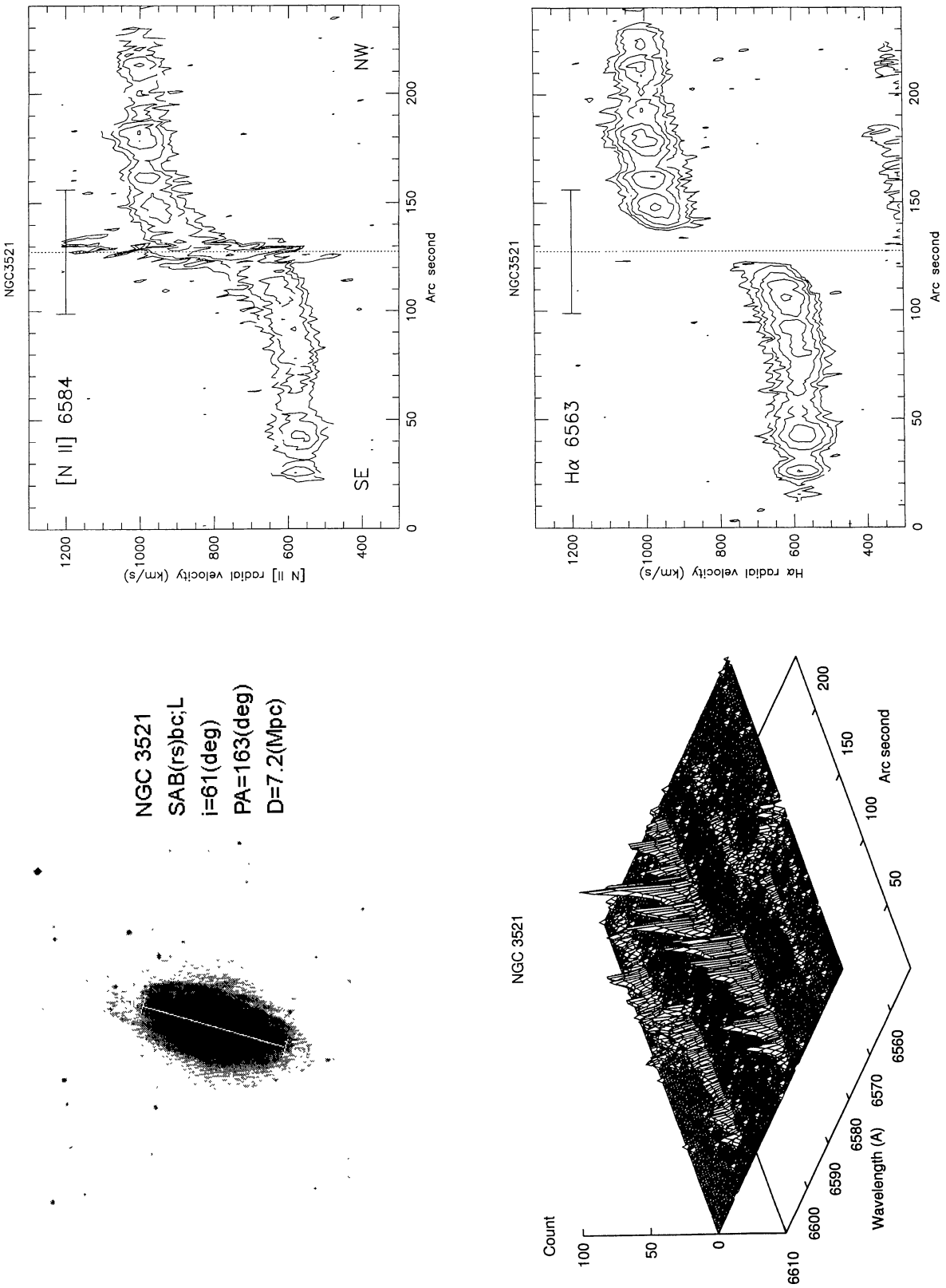

Fig. 1. Continued.

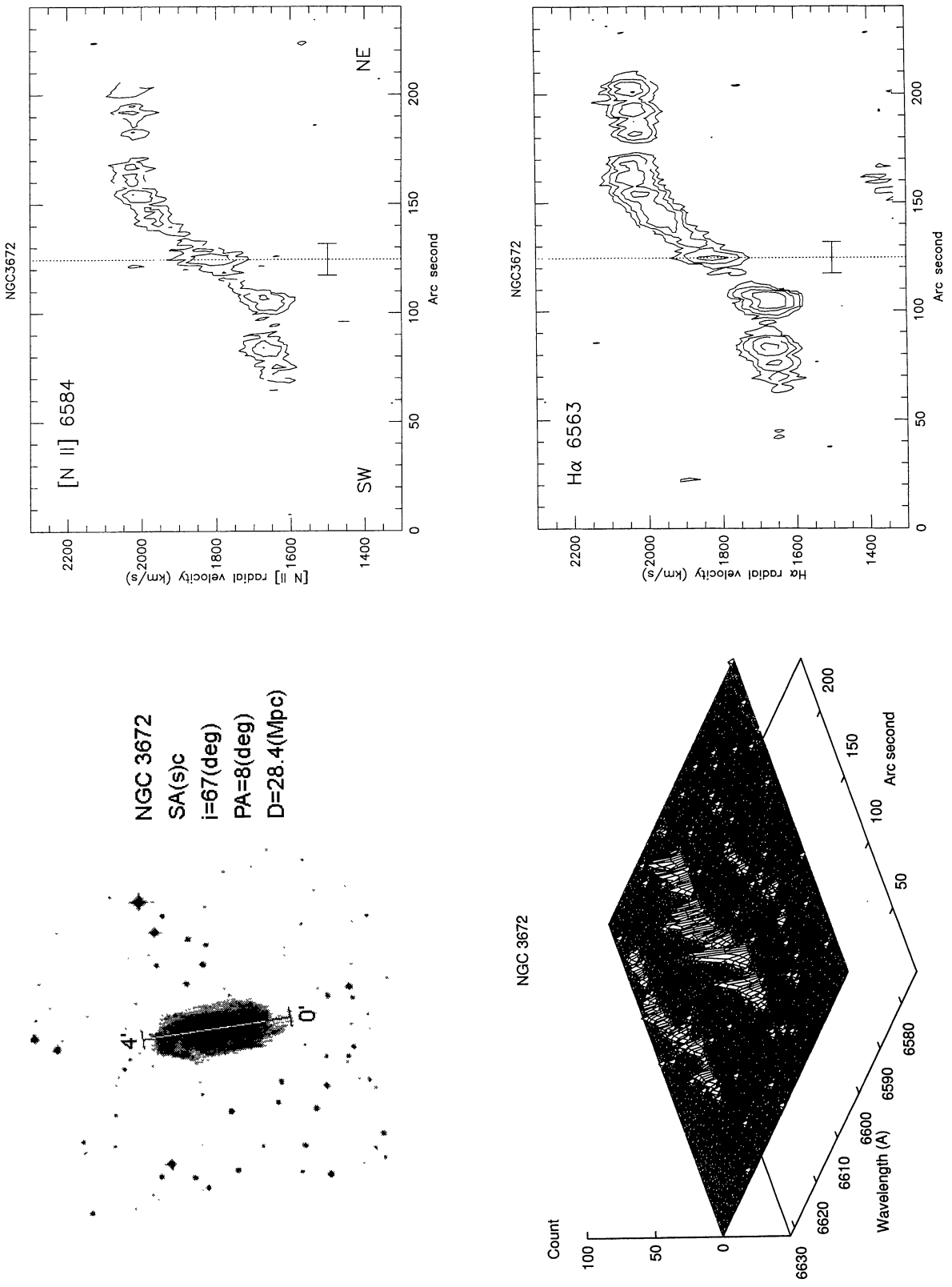

Fig. 1. Continued.

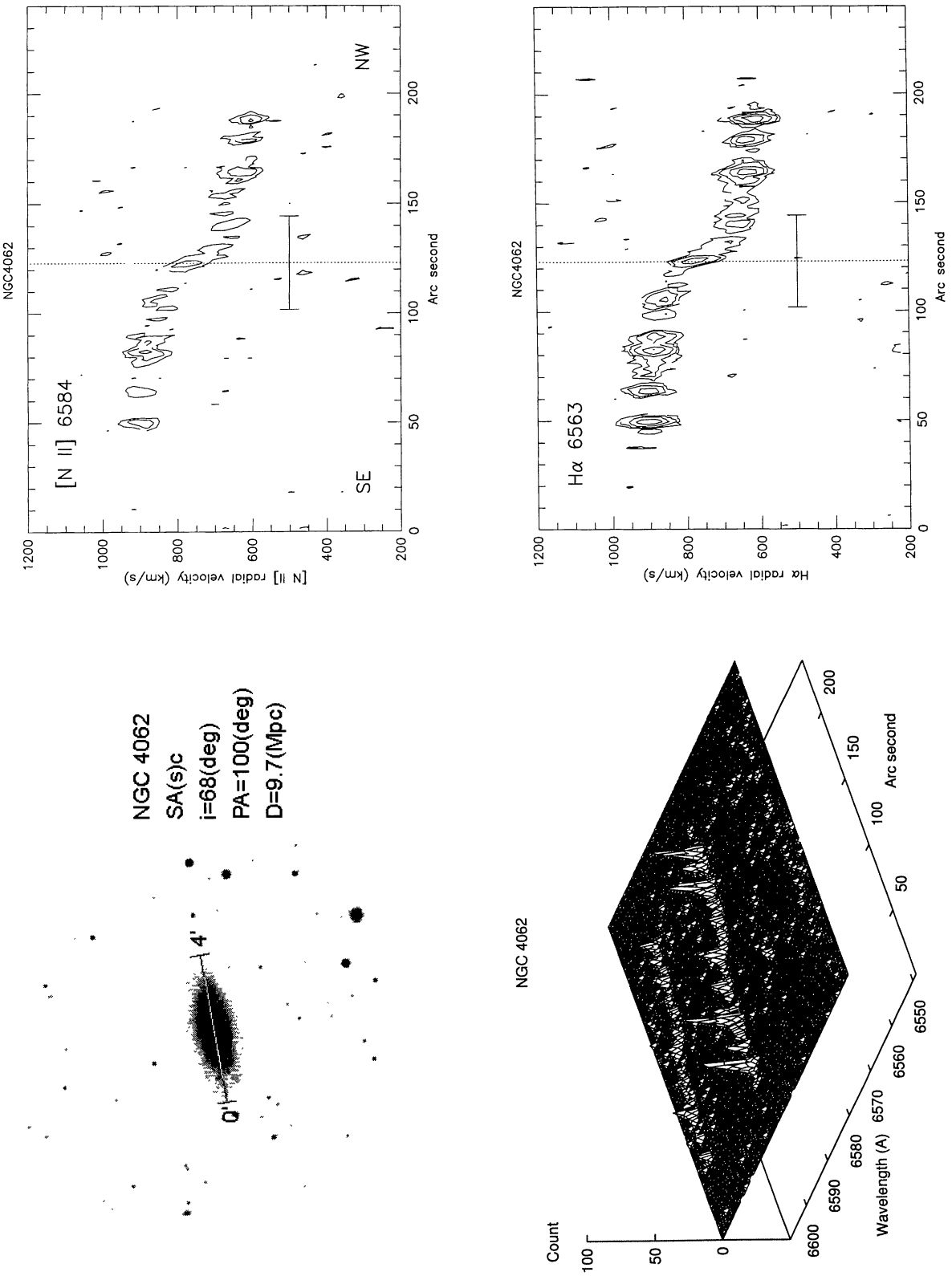

Fig. 1. Continued.

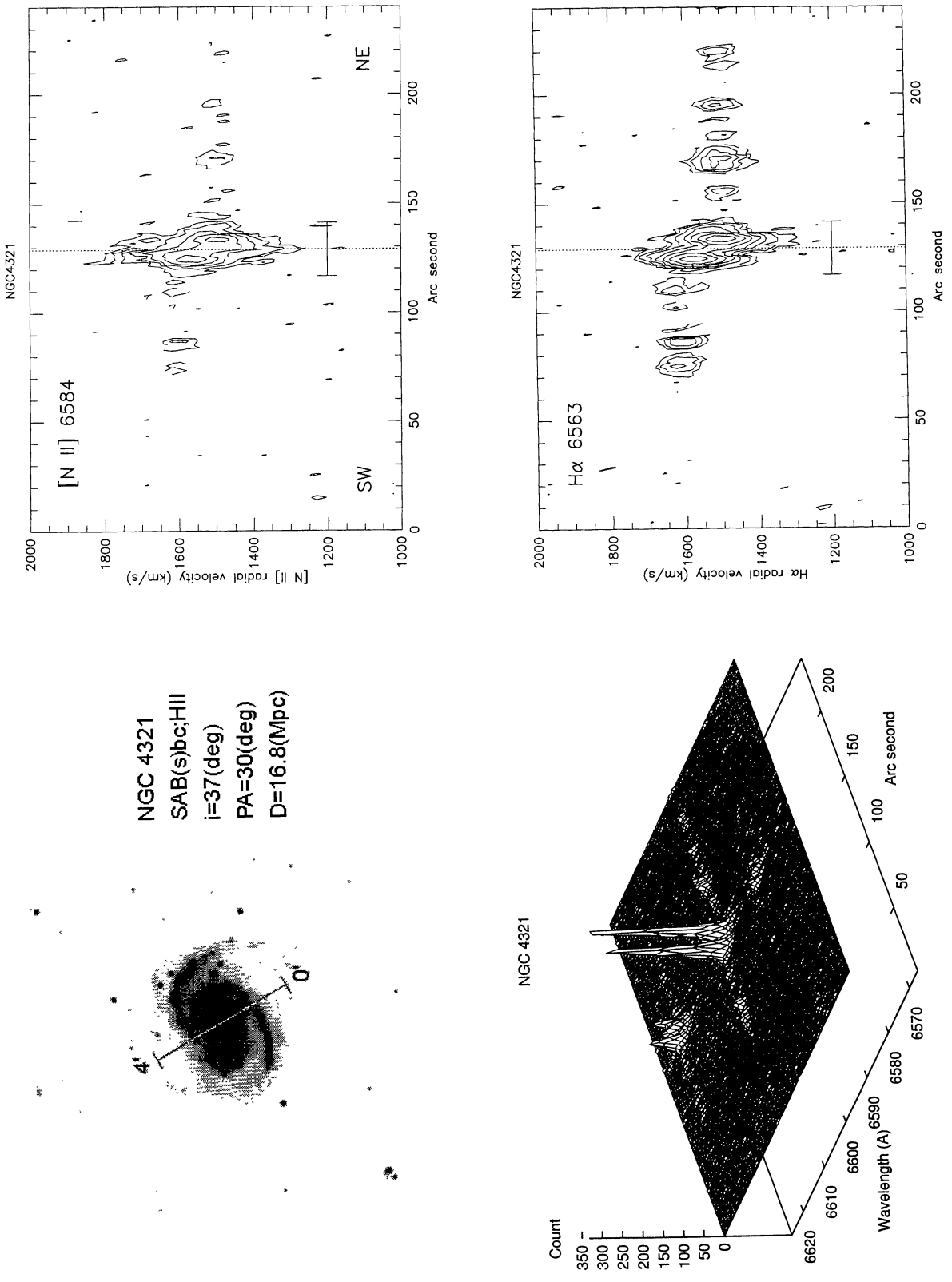

Fig. 1. Continued.

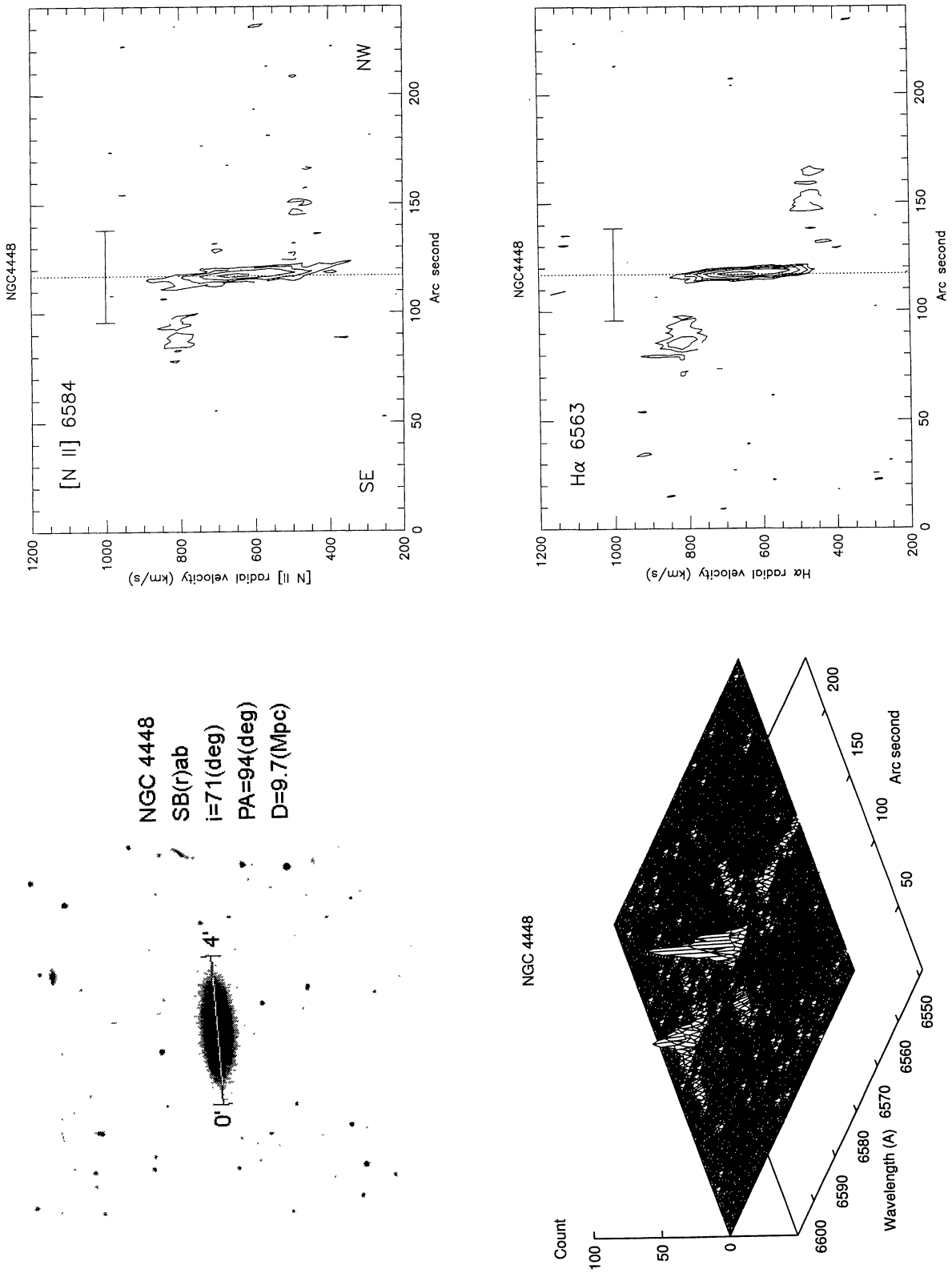

Fig. 1. Continued.

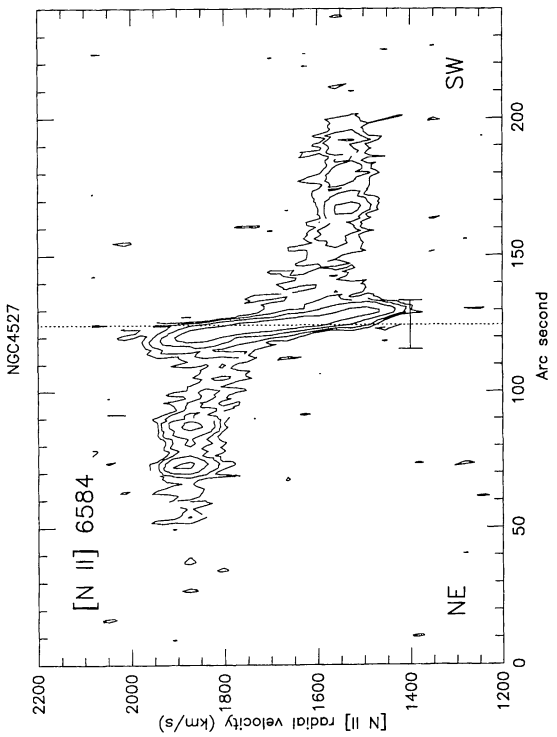

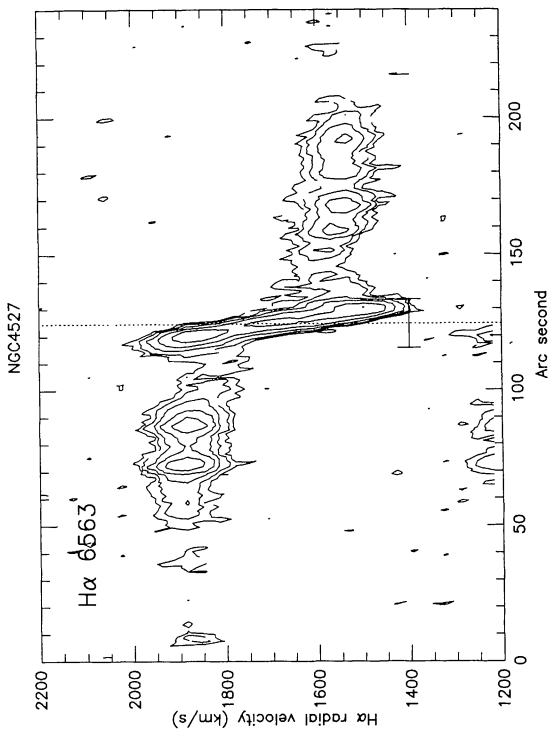

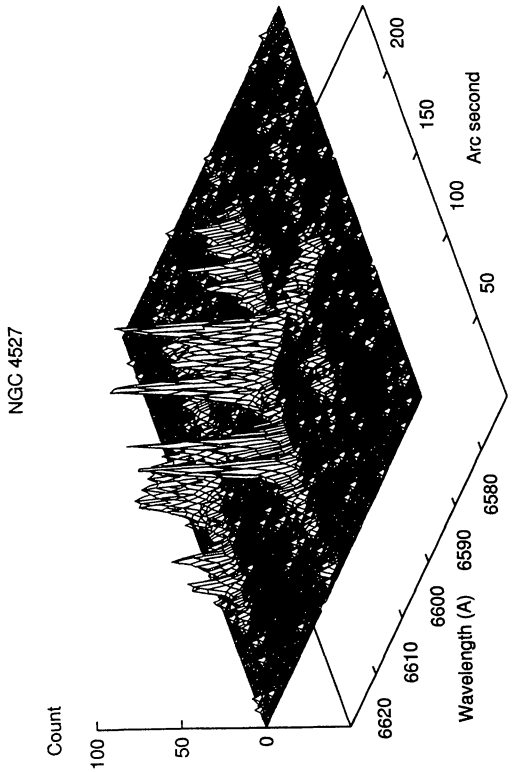

Fig. 1. Continued.

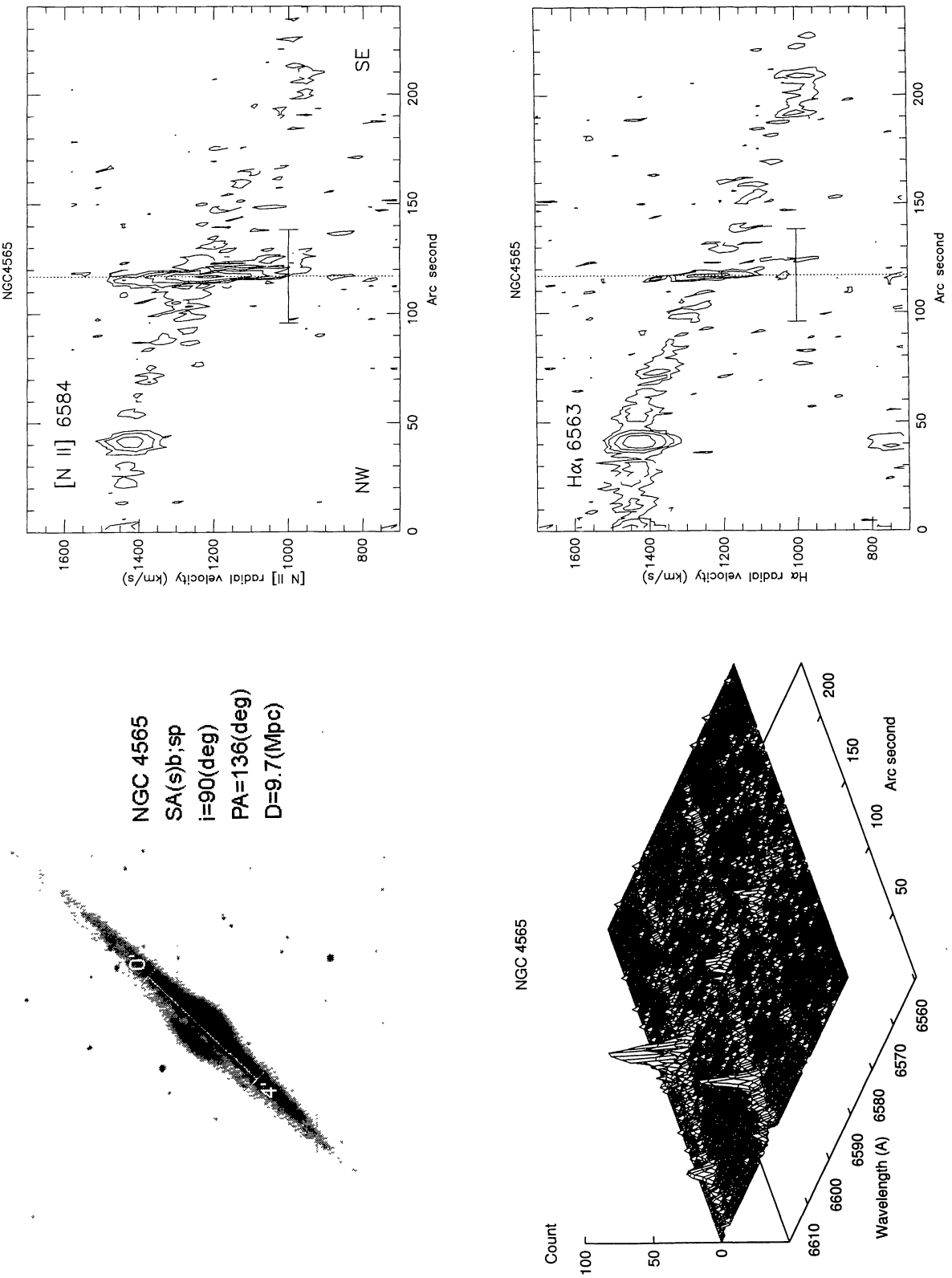

Fig. 1. Continued.

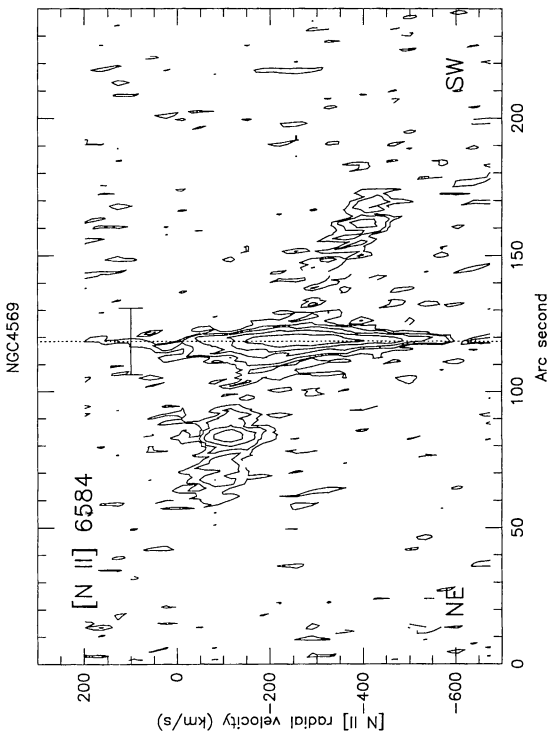

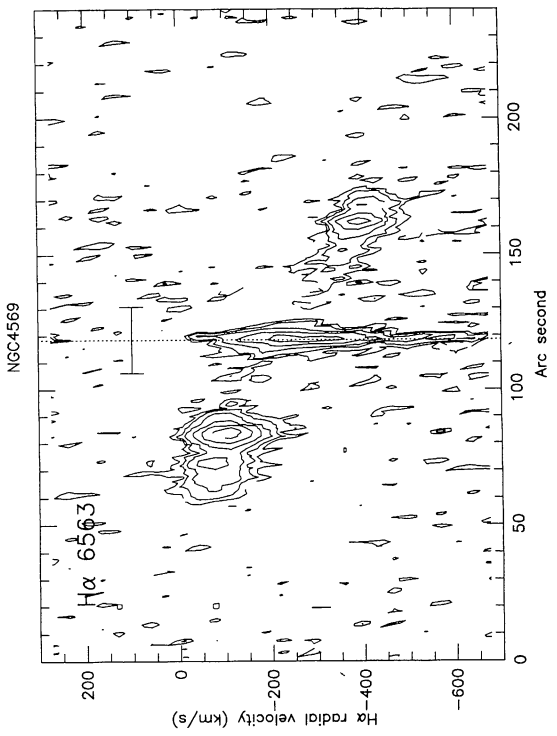

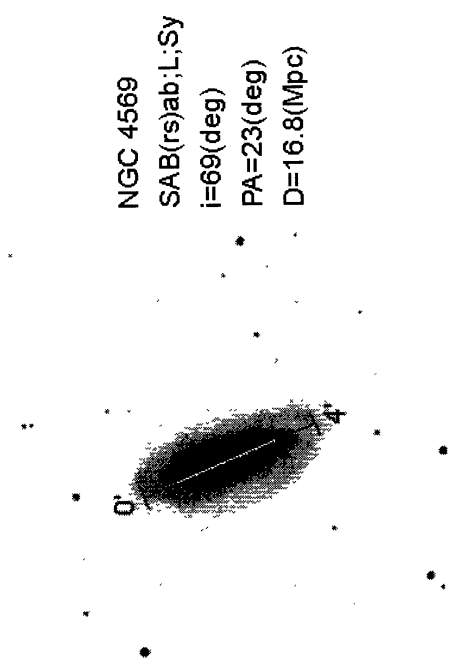

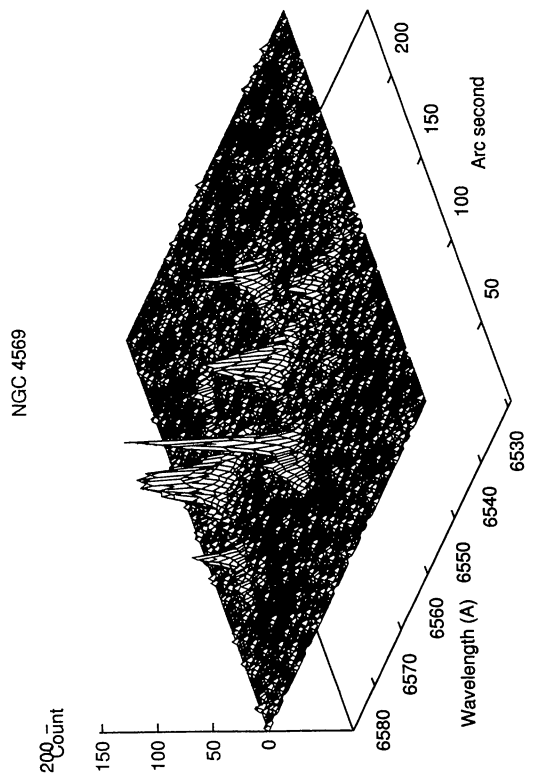

Fig. 1. Continued.

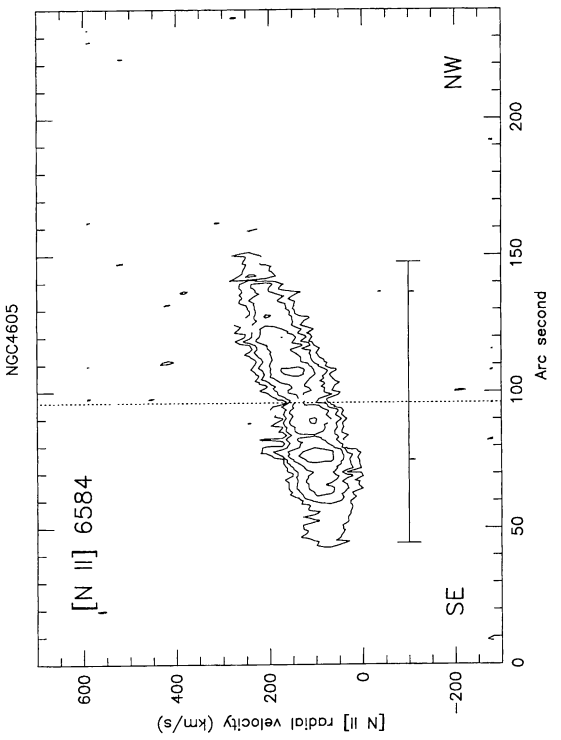

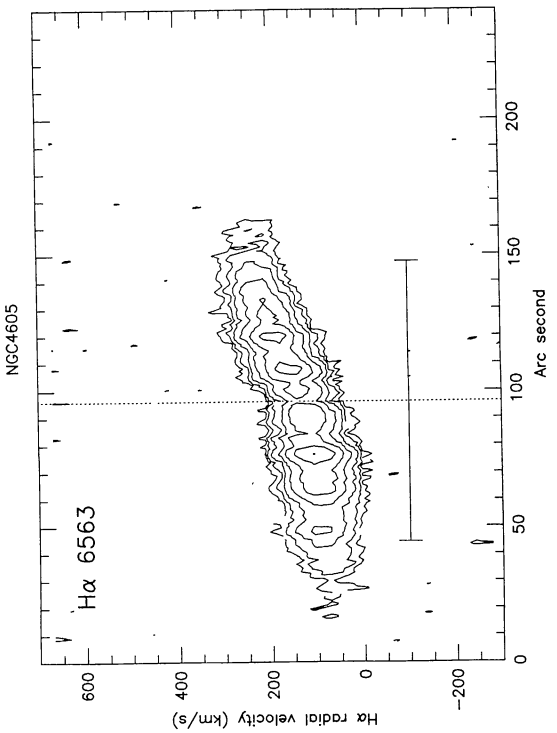

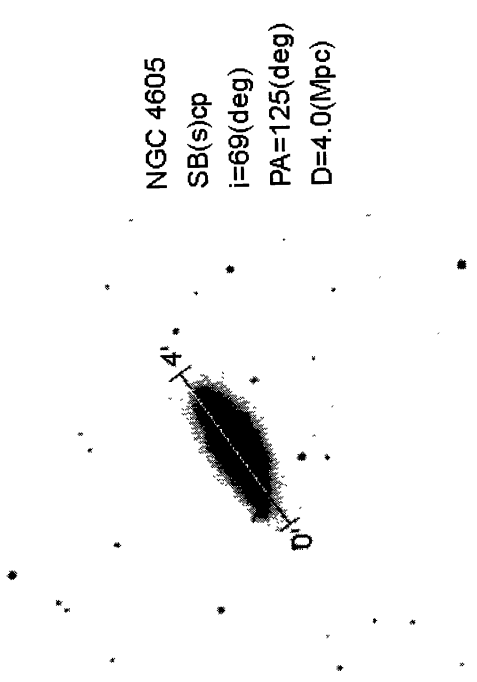

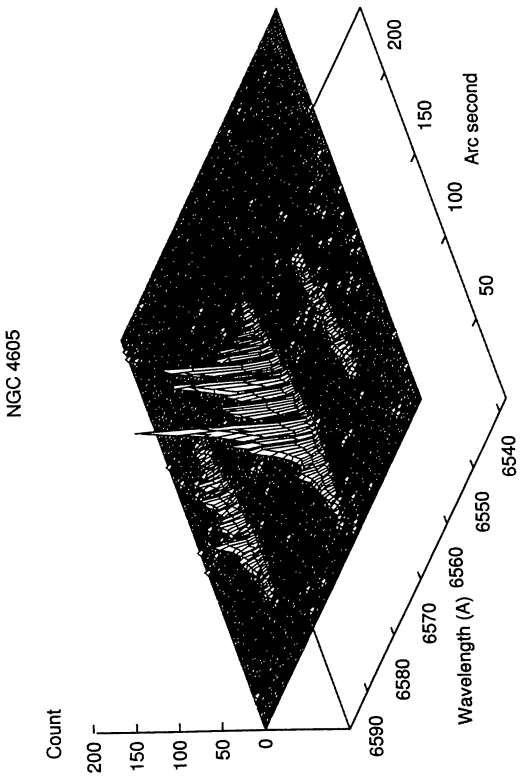

Fig. 1. Continued.

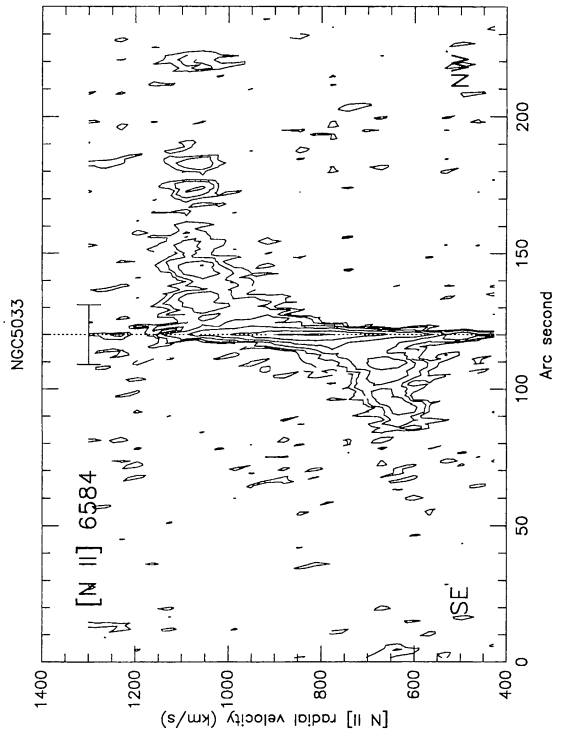

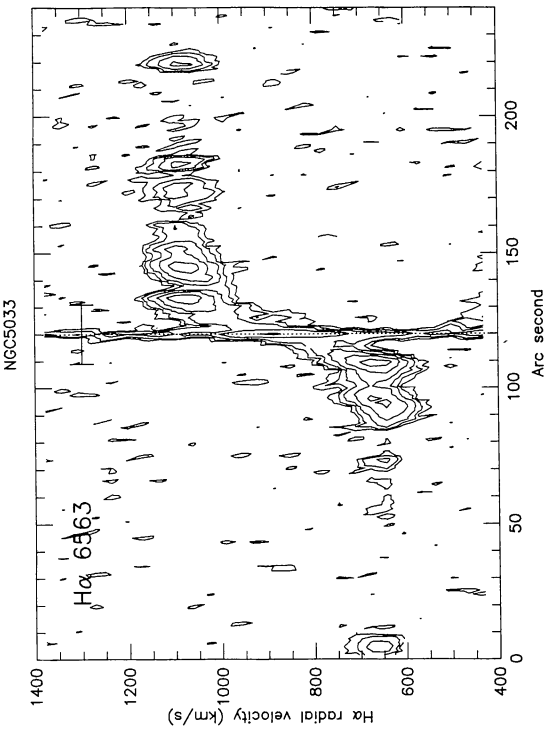

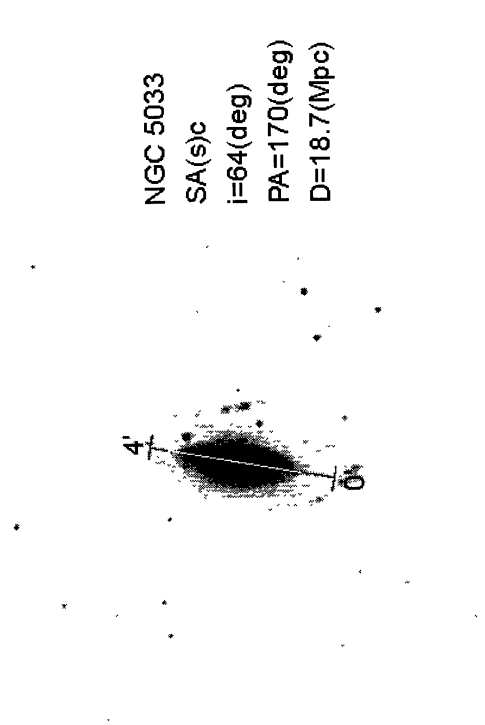

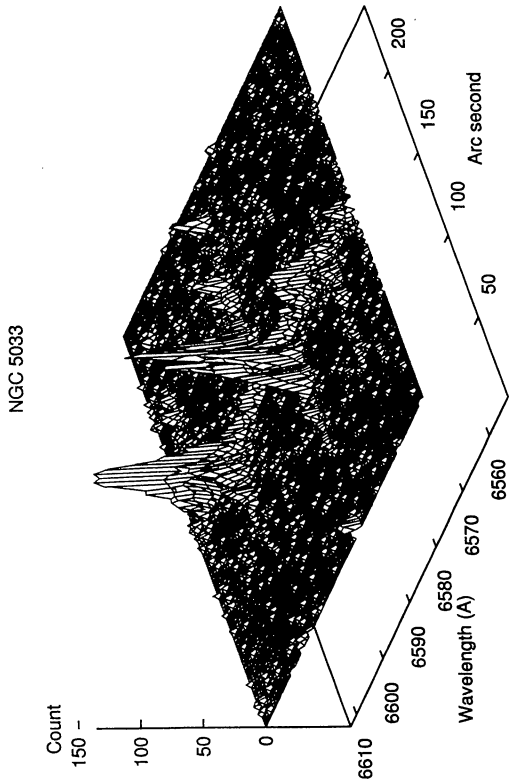

Fig. 1. Continued.

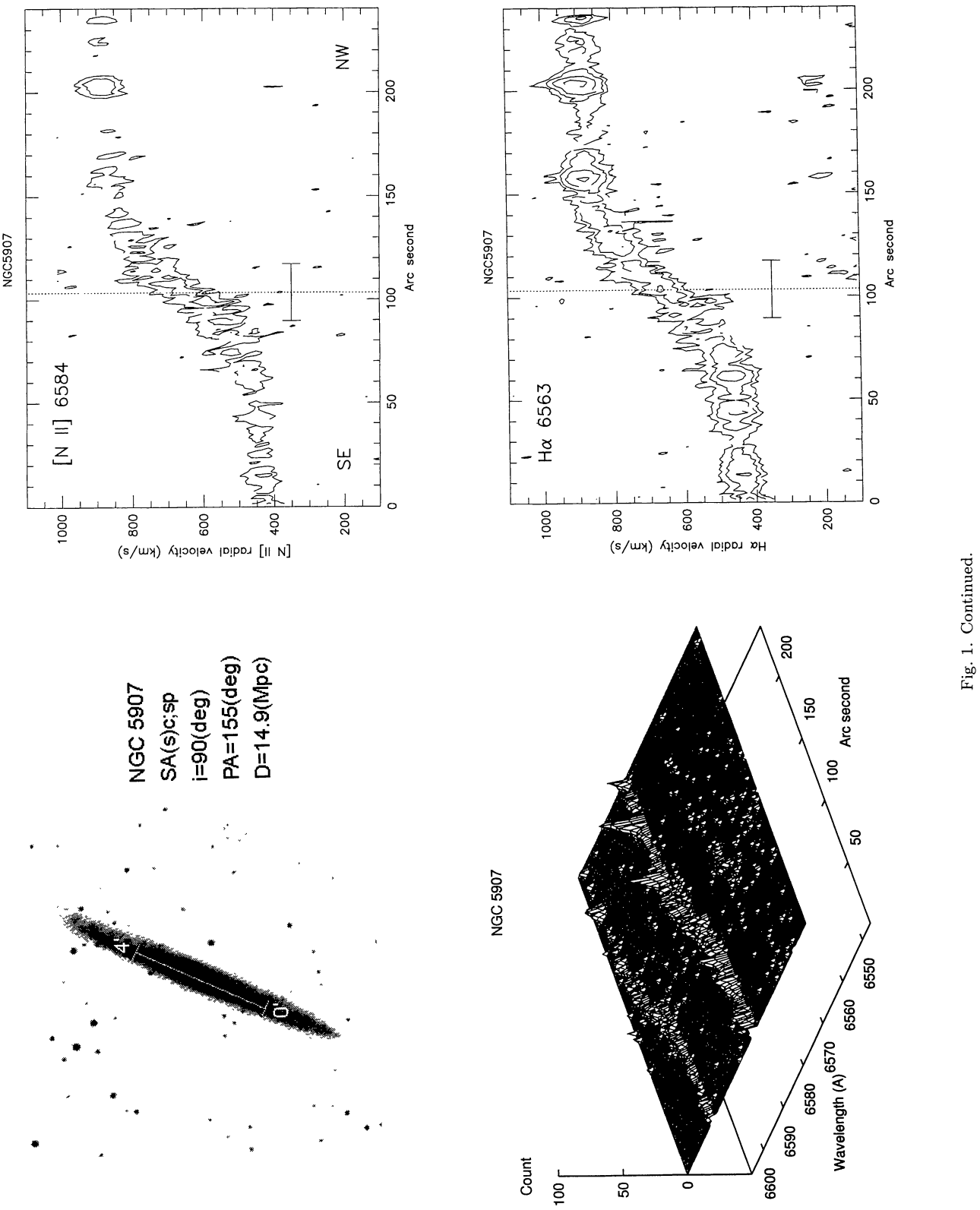

Fig. 1. Continued.

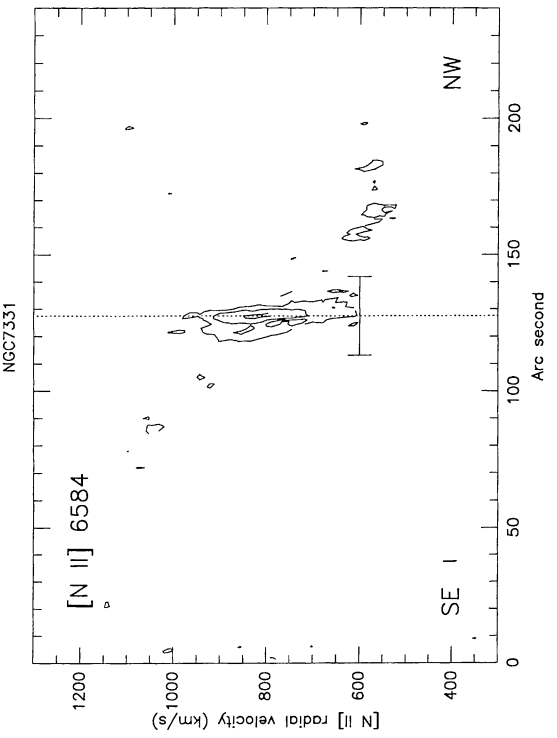

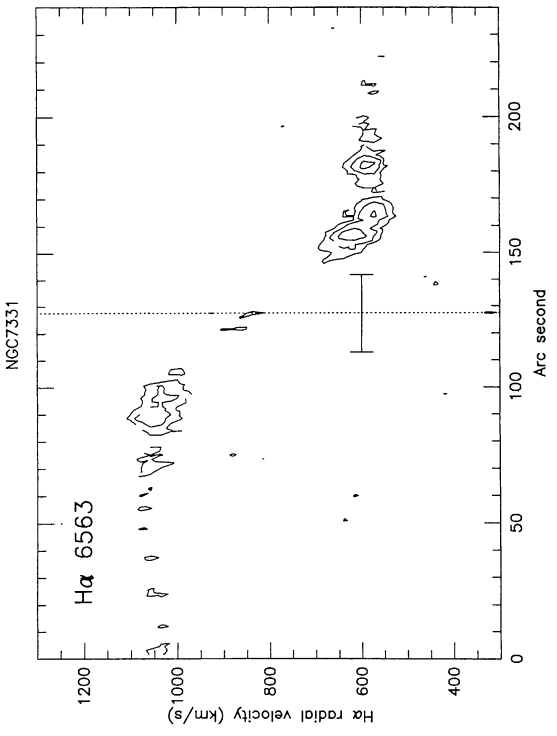

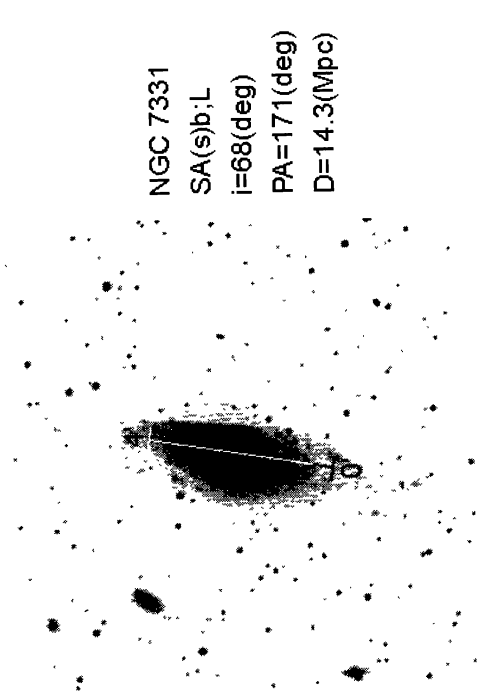

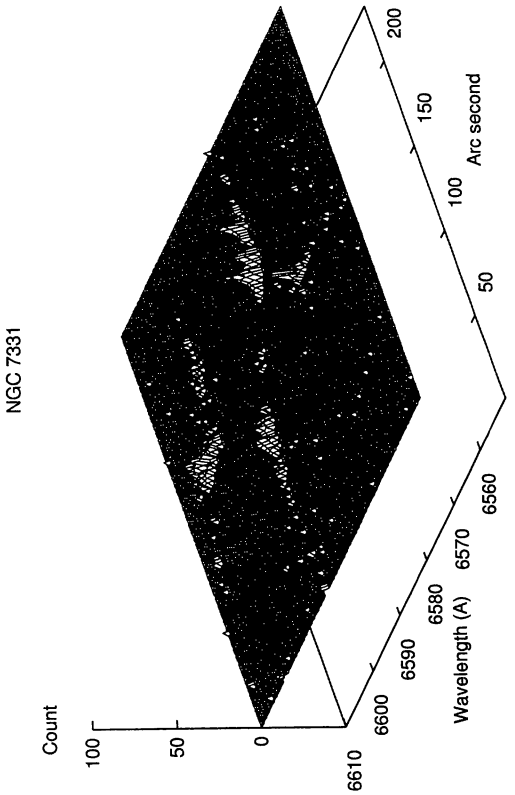

Fig. 1. Continued.

candidates of the central position of the galaxy. Constructing a histogram based on these data, we could reasonably well establish the position of the galaxy-center as being the most frequent value. The length of the horizontal short bar crossing this center-line shows the actual (physical) scale on the galaxy corresponding to 2 kpc (i.e., extension of ± 1 kpc from the galaxy center), which was evaluated by using the redshift-based distance (D) given in table 1.

Except for a few cases, the PV diagrams are characterized by two components: a bright nuclear component with a large velocity gradient and/or dispersion, indicating a rapidly rotating nuclear disk, and a flat component showing a nearly constant rotation in the disk and outer region.

3.2. Line Profiles

The left lower panels of figure 1 show the spectral profiles of the Hα and [N II] lines at individual positions on the major axis, drawn in the form of a three-dimensional plot. The abscissa is the wavelength (radial velocity) and the ordinate is the distance along the major axis. For the purpose of background-smoothing, which helps to clarify the emission feature of present interest, any value (irrespective of positive or negative) below the threshold level of 3 counts was intentionally set to zero. These plots can be used to compare the line profiles of the Hα and [N II] lines, whose shapes show complicated variations near to the nucleus.

In the disk regions, the Hα-to-[N II] line intensity ratio (HNR) is usually equal to about three, which is typical for H II regions (e.g., Osterbrock 1989) and the two lines show almost the same profiles. The Hα line profile of the nuclear component often shows a double-horn feature, representing an unresolved rotating disk. However, the nuclear Hα emission is sometimes superposed by a broad stellar absorption lines, likely to be due to the Balmer wing of A type stars, such as in the case of NGC 3521, in which no emission feature is recognized any more, being merged by a broad, strong absorption.

Some galaxies, like NGC 5033, shows a superposition of a broad Seyfert emission feature on the Hα line. Thus, the Hα PV diagrams and line profiles very close to the nucleus are often deformed from the pure emission features, which may cause pseudo-kinematical properties. On the other hand, the [N II] line is not affected by such a stellar absorption feature or by the Seyfert broad emission, though the signal-to-noise ratio is poorer than that of the Hα line by a factor of about two. Considering that the reconstruction processes of the Hα PV diagram contain uncertainty, it may be safer to use the [N II] line in the very central regions where the lines have sufficient signal-to-noise ratios.

4. Rotation Curves

4.1. Velocity Curves from the Centroid Wavelengths

We first derive velocity curves using the centroid of the wavelengths of the Hα 6563 and [N II] 6583 emission lines at each spatial position. Figure 2 shows the results, where the filled circles indicate data for Hα 6563, and the open circles that for the [N II] 6583 line. The vertical dotted-line and the horizontal bar have the same meaning as in the case of the contour diagrams in figure 1.

We define the radial velocities as follows: In a one-dimensional spectrum, $s_m(n)$ at each spatial position m, with s being the intensity, n the wavelength or pixel number in the direction of dispersion, the position of emission peak n_0, which is defined as that satisfying the following conditions simultaneously, was detected automatically by using a small program. (i) $s(n_0-2) < s(n_0-1)$ and $s(n_0-1) < s(n_0)$ and $s(n_0) > s(n_0+1)$ and $s(n_0+1) > s(n_0+2)$. (ii) $s(n_0)$ is above the (assumed) threshold level of 5 counts. Such a determined peak position can be directly converted to the (peak) radial velocity. However, the resulting plots were unsatisfactory because of the finite size of the pixels; i.e., something like discontinuously assembled line-segments, rather than a continuous curve.

We, therefore, decided to use the centroid wavelength instead of the peak wavelength. Once the peak wavelength position, n_0, is established, it is easy to find the two wavelength positions corresponding to the half-maximum intensity, $s(n_0)/2$ by an appropriate interpolation. Let these two values be n_- and n_+ (the inequalities of $n_- < n_0 < n_+$ hold), respectively. Then, the centroid wavelength of the emission line is defined as the mean of n_- and n_+, i.e., $(n_- + n_+)/2$. The rotation curve constructed by using the radial velocity corresponding to such a mean-wavelength at half-maximum turned out to be more continuous and natural to the eyes, which may thus be more preferable compared to the peak-velocity curve.

4.2. Rotation Curves from the Envelope-Tracing Method

We next derive rotation curves from the PV diagrams by applying the envelope-tracing method (Sofue 1996). The velocity dispersion of the interstellar gas ($\sigma_{\rm ISM}$) and the velocity resolution of observations ($\sigma_{\rm obs}$) are corrected for as follows: The correction for the finite-velocity resolution $\sigma_{\rm obs} = 0.5$ FWHM (full width of half maximum) is given by

$$\sigma_{\rm cor} = \sigma_{\rm obs} \exp[-(d/\sigma_{\rm obs})^2]. \quad (1)$$

Here, d is the velocity difference between the maximum-intensity velocity near to the profile edge and the half-maximum velocity (half width of the intensity slope at

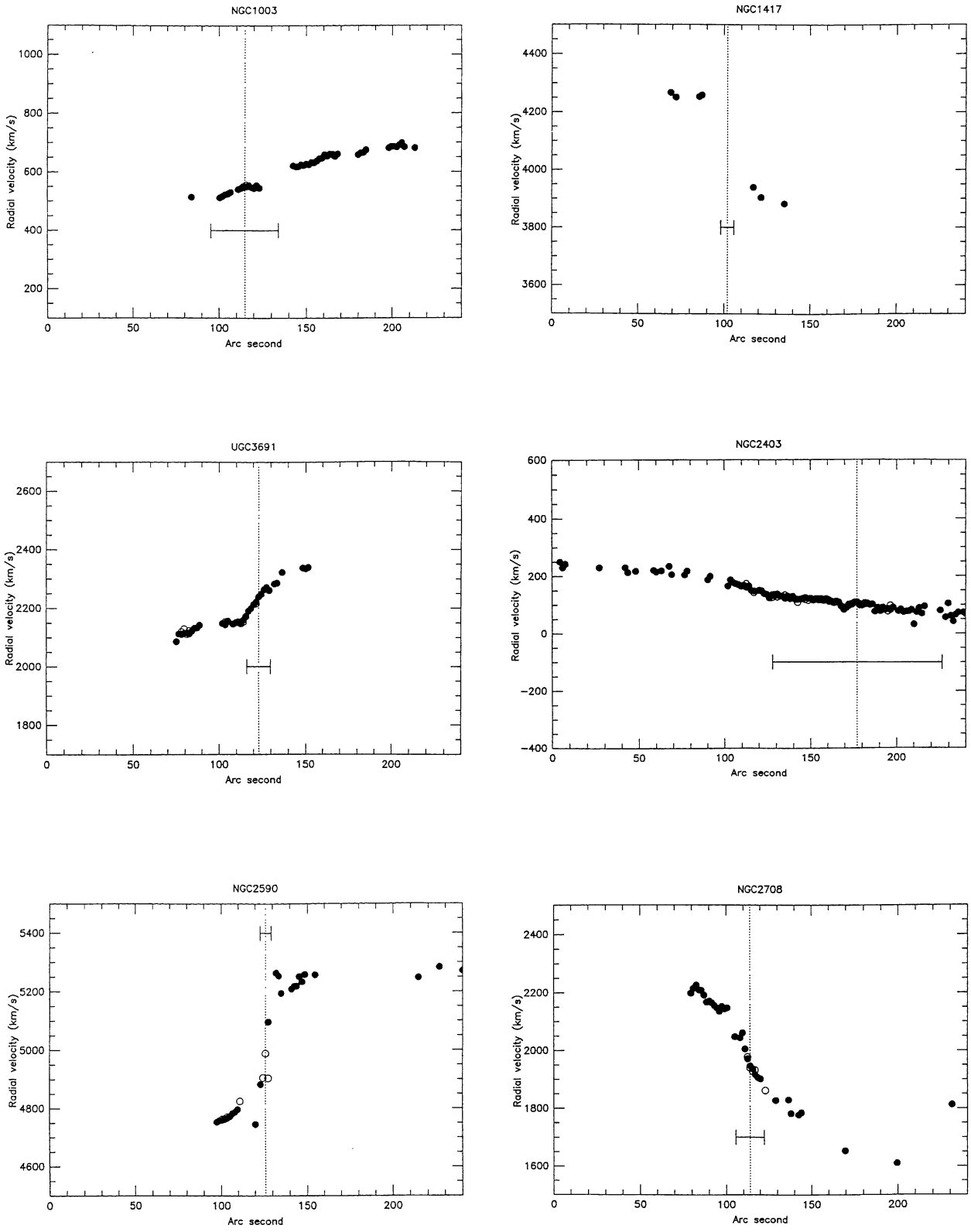

Fig. 2. Velocity curves derived using the centroid of wavelengths from the PV diagrams in the Hα and [N II] line emissions. The filled circles indicate data for Hα 6563, and the open circles those for the [N II] 6583 line. The vertical dotted-line and the horizontal bar have the same meaning as in the case of the contour diagrams in figure 1.

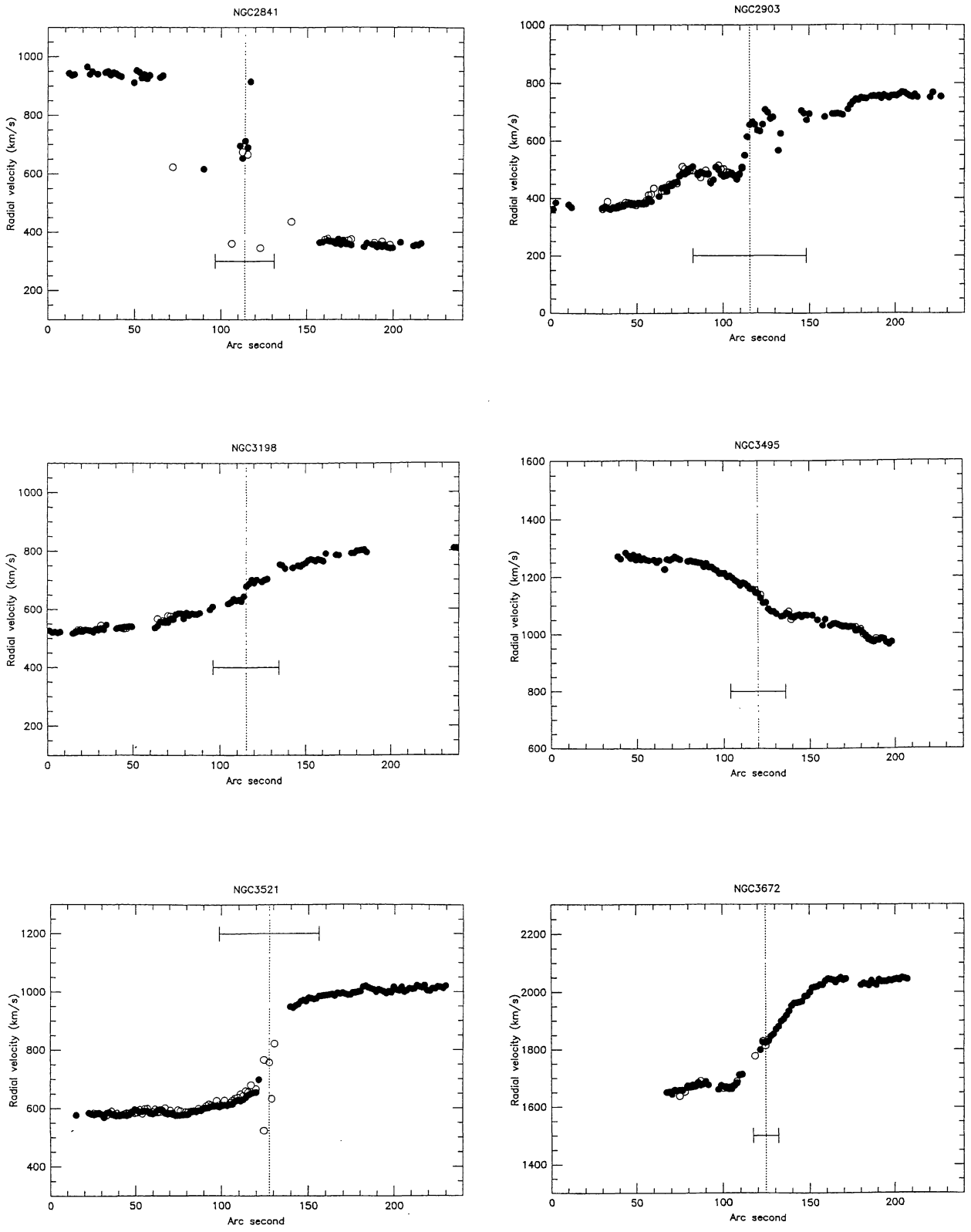

Fig. 2. Continued.

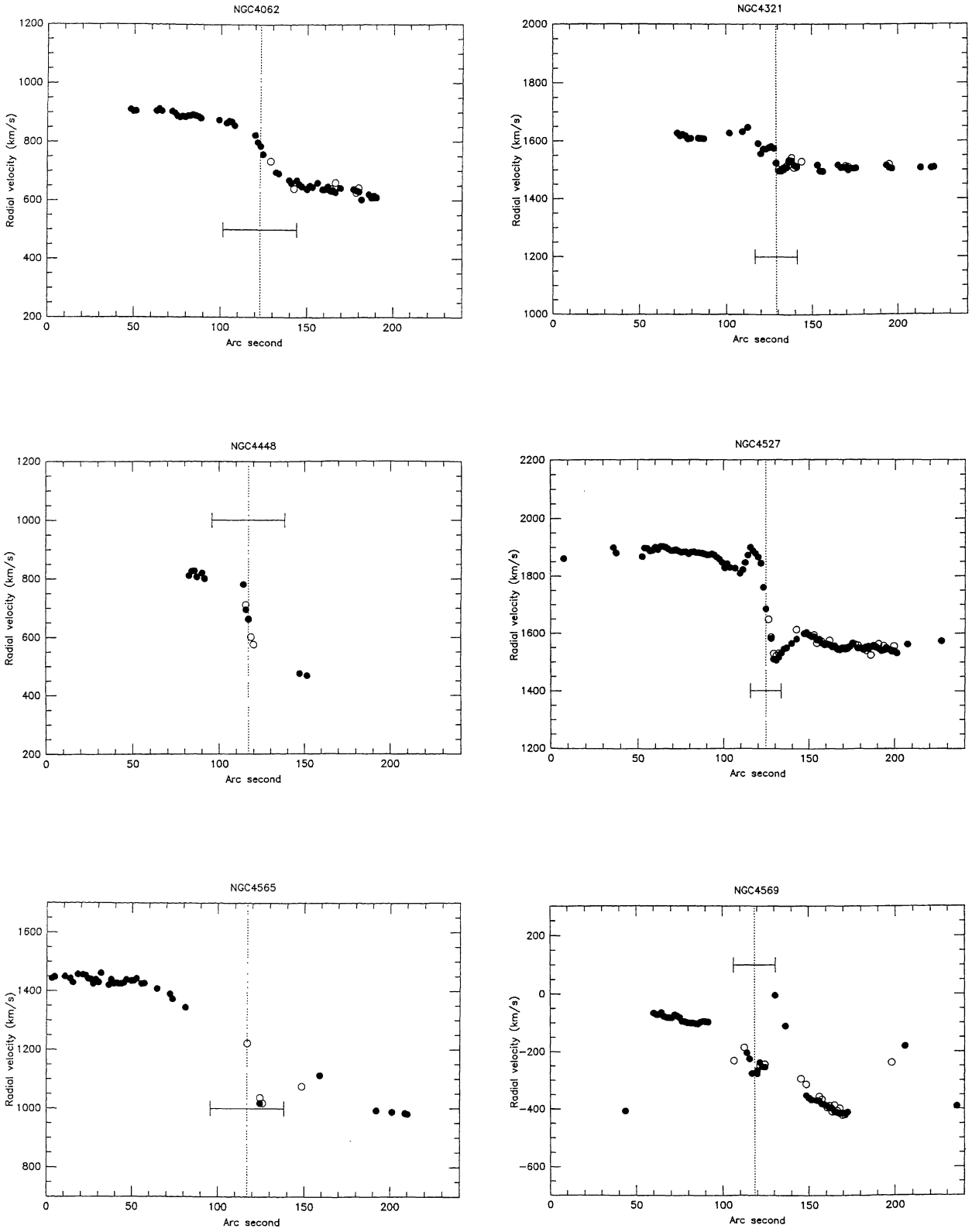

Fig. 2. Continued.

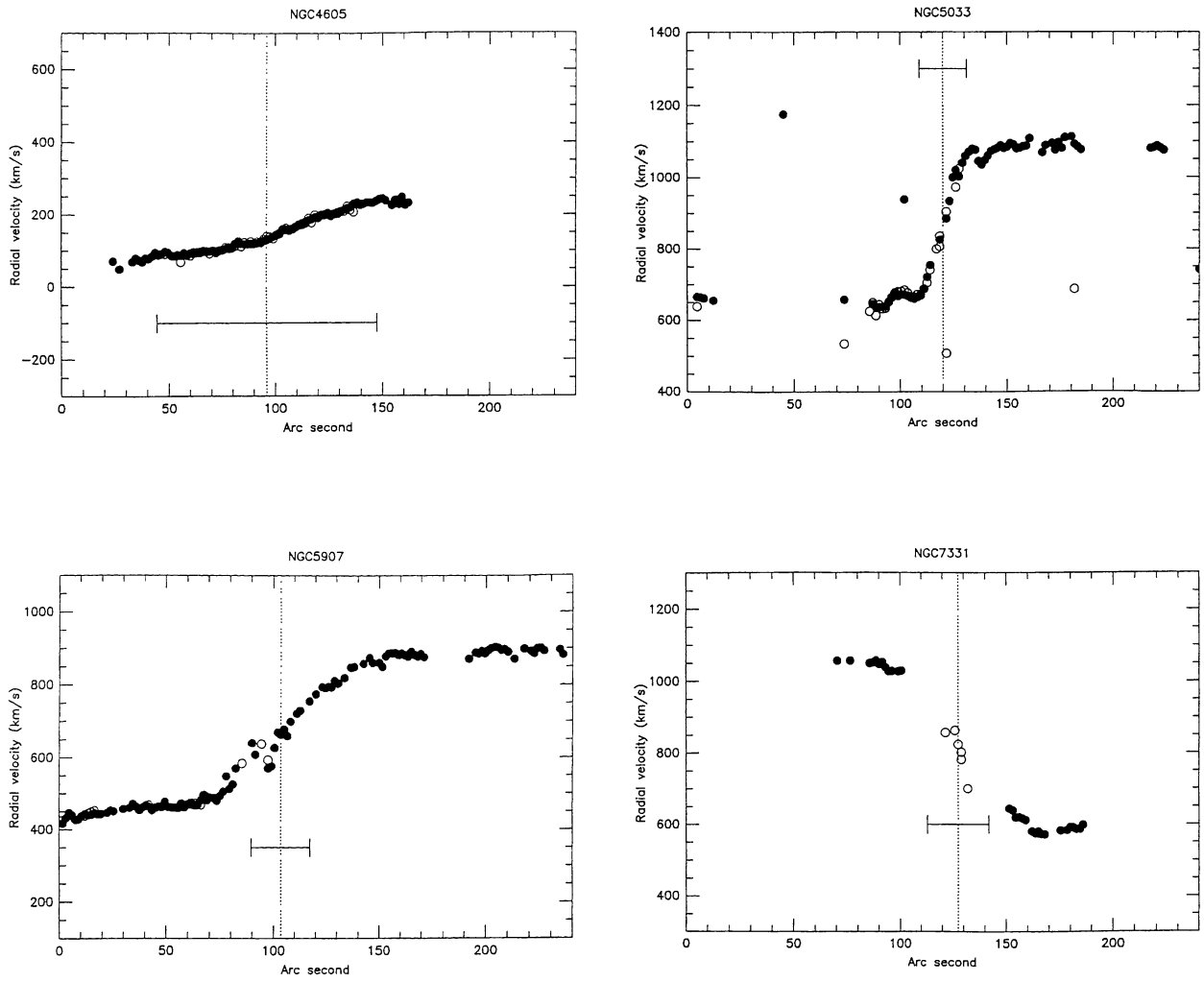

Fig. 2. Continued.

the velocity edge). Equation (1) implies that, if the original velocity profile of the source is sharp enough, the observed profile becomes the telescope velocity profile, so that the correction is equal to the velocity resolution ($\sigma_{\rm cor} = \sigma_{\rm obs}$). On the other hand, if the velocity profile of the source is greatly extended ($d \gg \sigma_{\rm obs}$), the correction becomes negligible ($\sigma_{\rm cor} \sim 0$) and the half-maximum velocity gives the rotation velocity.

The terminal velocity, $V_{\rm t}$, is defined by a velocity at which the intensity becomes equal to

$$I_{\rm t} = 0.5\ I_{\rm max} \tag{2}$$

on the PV diagrams. Then, the rotation velocity is estimated by

$$V_{\rm rot} = [V_{\rm t} - (\sigma_{\rm cor}^2 + \sigma_{\rm ISM}^2)^{1/2}]/\sin i. \tag{3}$$

For the Hα and [N II] lines in the present observations, we take $\sigma_{\rm ISM} \sim 7$ km s^{-1} and $\sigma_{\rm obs} = 87/2 = 43.5$ km s^{-1}. The error in estimating the rotation velocity is ± 10 km s^{-1} for regions with a sufficient signal-to-noise ratio, e.g., in the central regions and the disks. The obtained rotation curves for the Hα and [N II] data are shown in figure 3 with the abscissa in kpc. The inserted horizontal bar indicates the angular scale of 30″ on the sky. The distances to the galaxies have been adopted from table 1, column 9 (calculated by $H_0 = 75$ km s^{-1}), except for galaxies with redshifts smaller than 200 km s^{-1}, for which the Tully–Fisher distances have been adopted from column 10 of table 1. Figure 4 plots all of the obtained rotation curves in the same panel.

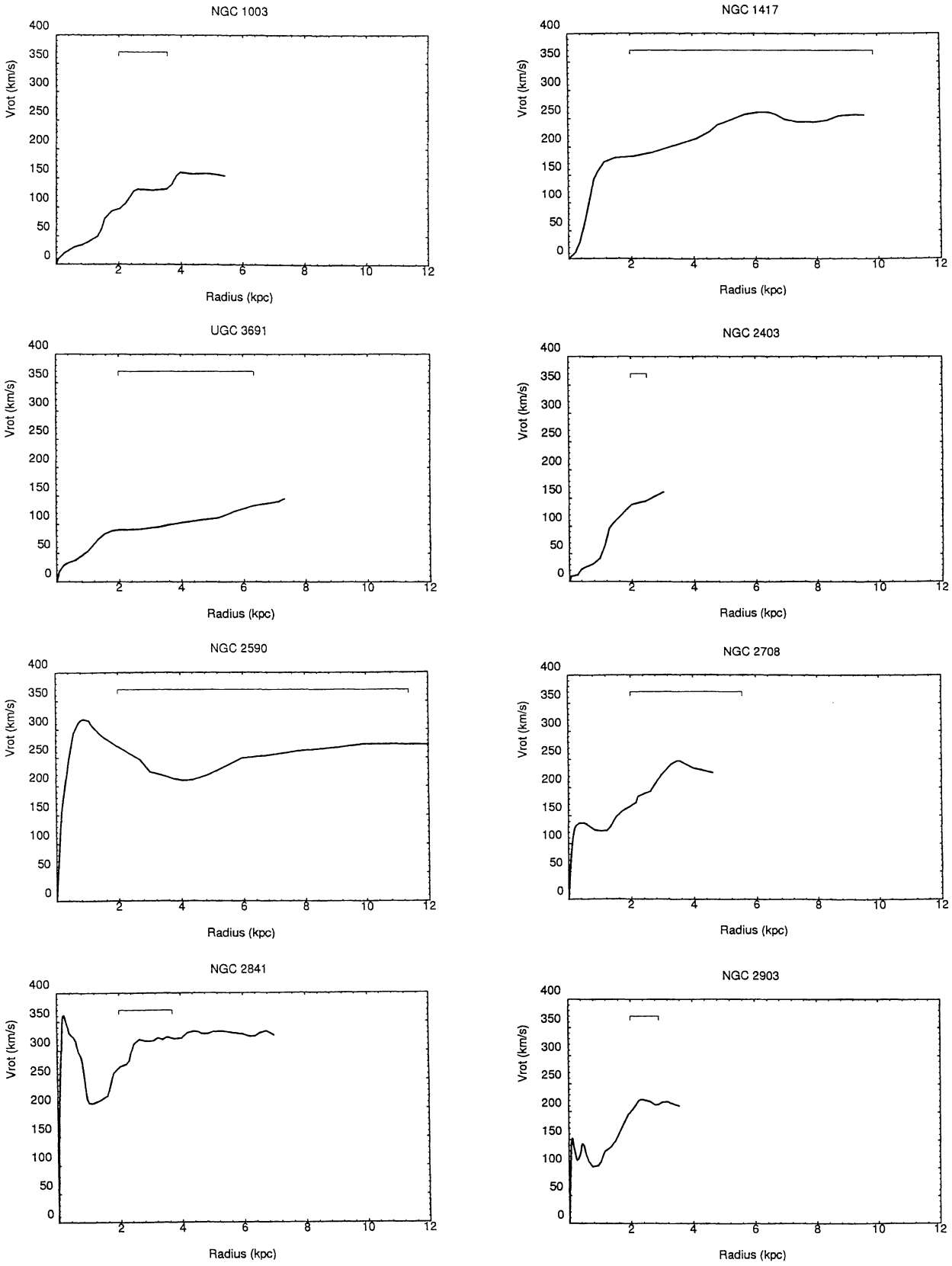

Fig. 3. Rotation curves derived from the PV diagrams using the envelope-tracing method, plotted against the radius in kpc. The horizontal bars indicate an angular length of 30″ on the sky.

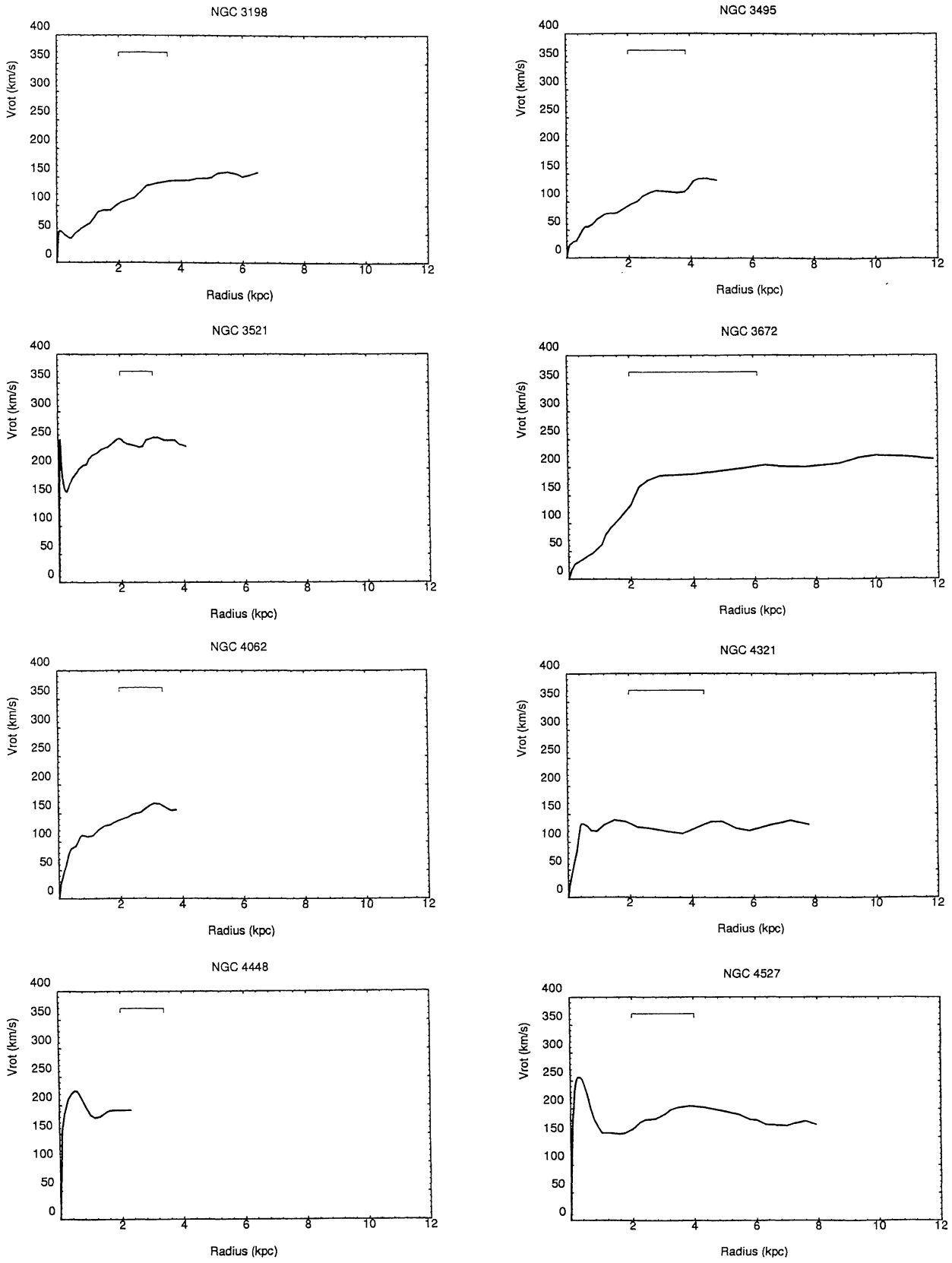

Fig. 3. Continued.

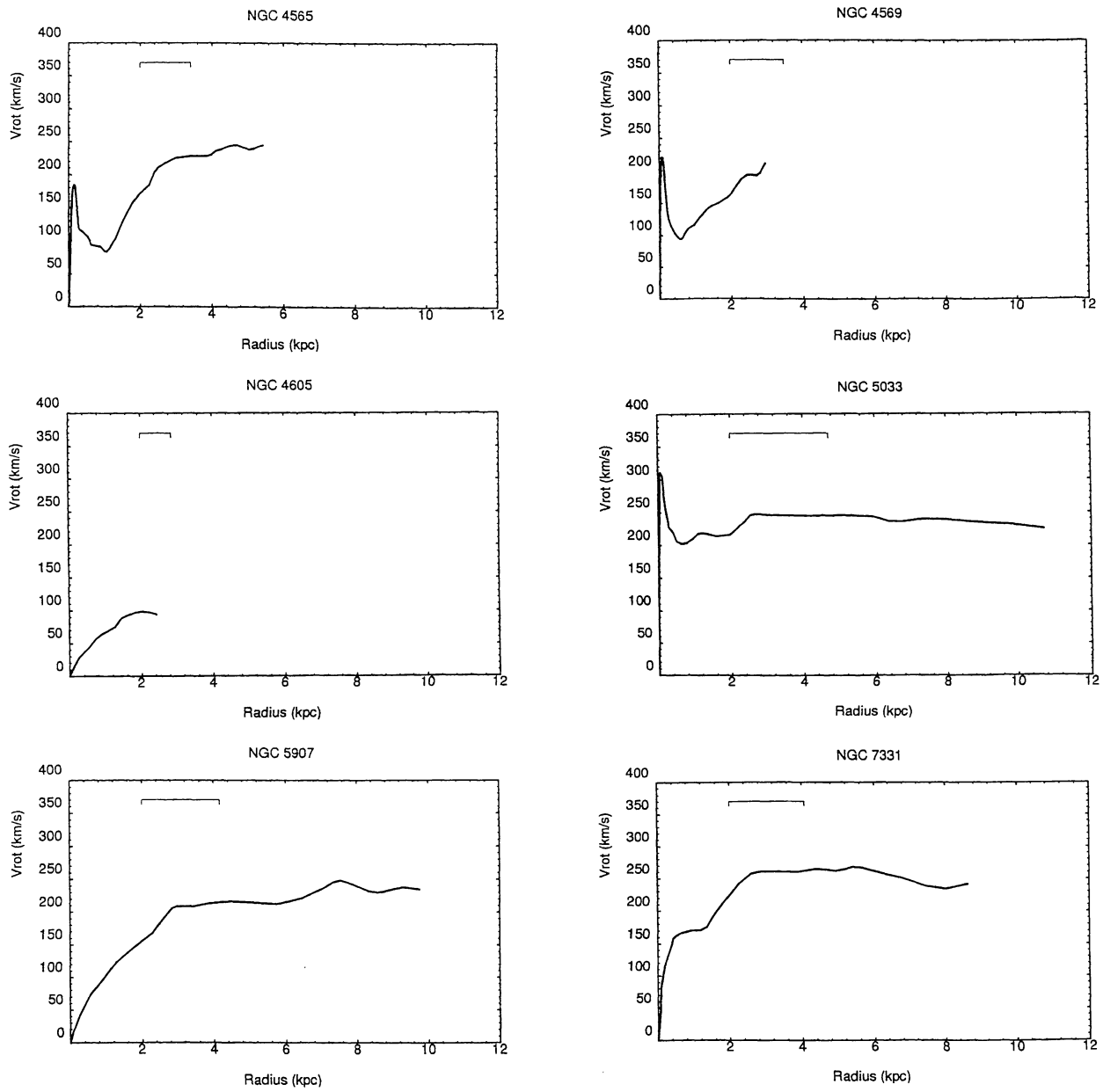

Fig. 3. Continued.

5. Description of Individual Galaxies

NGC 1003: This is a highly-tilted Sc galaxy, having a slow rotation. The nuclear component is not visible. The PV diagram shows a strong asymmetry, with a bright H II region being present at 20″ east of the nucleus.

NGC 1417: Since the data are noisy, the PV diagram shows only a flat disk component at both sides of the nucleus. No nuclear component is visible in the present data, probaby due to the poor data quality.

UGC 03691: No clear nuclear component is visible in the PV diagram. The rotation curve rises rapidly in a rigid-body fashion, reaching a flat rotation at $R \gtrsim 20''$.

NGC 2403: This Sc galaxy has a morphology similar to the nearby Sc galaxy M33, showing amorphous spiral features. The PV diagram shows an almost rigid-body rotation at $R < 50''$, with a larger gradient in the central $\pm 10''$. The rotation curve is similar to that of M33. The disk rotation is almost flat, but it still appears to gradually increase toward the observed edge. The Hα-to-[N II] line intensity ratio (HNR) is as large as ~ 5

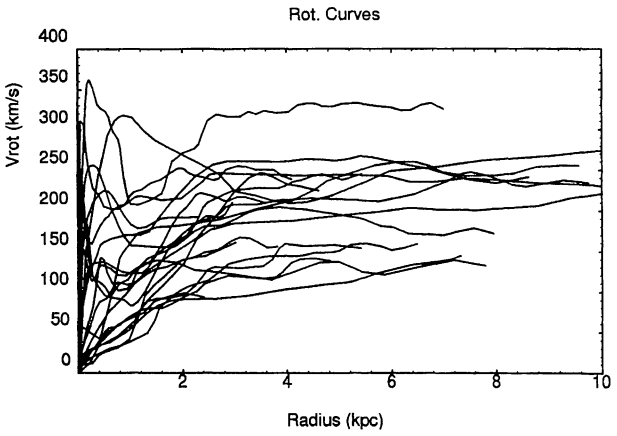

Fig. 4. Same as figure 3 but plotted in the same panel.

at the nucleus, slightly larger than the normal value of about three for the H II regions.

NGC 2590: This Sbc galaxy shows a high-velocity nuclear disk with a rapidly increasing rotation at $R < 2''$ (600 pc), followed by a flat rotation until $R \sim 50''$ (16 kpc). The nuclear Hα disk is brighter than the disk part (figure 2), and the rotation property is similar to that of NGC 4527 (Sofue et al. 1998). The HNR at the nucleus is close to the value of normal H II regions. Since the distance is as large as 64.5 Mpc, no detail can be seen from the present data.

NGC 2708: The HNRs in both the disk and nuclear region are equal to about three, typical for H II regions. The PV diagram shows a typical nuclear rise, followed by a flat rotation in the disk.

NGC 2841: The nuclear component has an inverse HNR as small as ~ 0.3, and the Hα-line width is smaller than [N II]. This may be due either to a superposed broad Hα absorption, or to stronger emission in [N II], such as due to a higher-temperature circum-nuclear gas. The [N II] nuclear component shows a high concentration of the gas. The nuclear PV diagram is slightly tilted in the sense of the galactic rotation, indicating a compact, rapidly rotating gas. The PV behavior of the disk part is flat in both the Hα and [N II] lines, with a normal HNR value for H II regions. The rotation velocity of this galaxy is as high as ~ 300 km s^{-1} in the disk, and reaches almost 350 km s^{-1} in the nuclear disk.

NGC 2903: The Hα and [N II] lines show an almost identical behavior both in the PV and intensity plots. The HNR is also normal, as for in the H II regions. The nuclear component shows tilted double peaks in the PV diagram, indicating a rotating ring of radius $4''$ comprising H II regions. After decreasing to a minimum at $R \sim 25''$, the disk rotation gradually increases until $R \sim 50''$; it then increases suddenly, with a step, to a maximum at $R \sim 70''$, followed by flat rotation. This step-like rotation may be related to its barred structure.

NGC 3198: This is a highly titlted SBc galaxy. The nuclear component shows a rapid increase of rotation within $2''$, while its rotation velocity is as small as 50 km s^{-1}. The rotation velocity, then, increases smoothly to a maximum at $R \sim 60''$, followed by flat rotation. The HNR value is for the H II regions, and remains nearly constant through the disk and the nuclear component.

NGC 3495: The nuclear component is weak both in Hα and [N II]. The PV diagrams show a rigid-body behavior at $R \lesssim 50''$, followed by a flat part in the outer disk. This apparently rigid-body rotation may be due to interstellar extinction by the disk at a high inclination.

NGC 3521: This highly tilted Sbc galaxy shows a strong and broad Hα absorption around the nucleus. The absorption feature is as wide as ~ 20 Å (~ 1000 km s^{-1}), and is extended for about $10''$, but shows little rotation. On the other hand, the [N II] line suffurs from no absorption, and can be better used for tracing the kinematics in the PV diagram. The nuclear component in the [N II] line indicates a rapidly rising rotation curve of the nuclear disk. The disk part shows a nearly flat rotation in both the Hα and [N II] lines.

For its very slow rotation and extended feature, the Hα absorption component is most likely caused by a stellar absorption line of the central bulge stars. Such a broad absorption line is well known for A type stars as the damped wing in the Balmar lines due to Stark broadening. In order that such a bright A type star cluster be present, a large-scale starburst may have occurred within the last 10^9 years (e.g., Dressler, Gunn 1983).

NGC 3672: The nuclear component shows a compact, slowly rotating core, followed by a rigid-rotation feature of the PV diagram. The rotation velocity attains a maximum at $R \sim 35''$, and then, it is almost flat. The HNR has a nearly constant value for H II regions.

NGC 4062: A weak nuclear component is visible both in the Hα and [N II] lines, indicating a slowly rotating compact disk. The rotation velocity reaches its maximum at $R \sim 15''$, beyond which the rotation is nearly flat.

NGC 4321: This Sc galaxy has a high concentration of Hα emission near to the nucleus, and the PV diagram has a tilted double-horn feature, representing a rotating ring of H II regions. However, the central region within a few arcsec is associated with a broader [N II] feature than Hα, representing a slightly tilted PV ridge, suggesting a more compact, rapidly rotating component with a steeply rising rotation curve. Except for this [N II] steep component, the HNRs in the nuclear and disk components are normal for the usual H II regions.

NGC 4448: A compact nuclear component is found in the Hα and [N II] PV diagrams, indicating a steeply rising rotation velocity. The Hα line appears to be superposed by a broad absorption feature, which may result in a

narrower velocity dispersion of Hα than [N II]. The [N II] nucear component shows a faster rotating feature than Hα. The disk part is rather weak, with both Hα and [N II] lines showing a flat rotation.

NGC 4527: Double peaked nuclear PV feature is clearly visible both in the Hα and [N II] line emissions, indicating a rapidly rotating disk of $R \sim 4''$. The [N II] PV diagrams show a broader, and more steeply rising component of rotation near to the nucleus within the central $\sim 2''$. The rotation veocity then decreases to a minimum at $R \sim 15''$, and increases to a flat part from $R > 25''$. A detailed analysis of the PV diagrams and CO line data is presented in Sofue et al. (1998).

NGC 4565: This is an edge-on galaxy of Sb type. The nuclear component is weak in the Hα emission, while being rather strong in [N II]. This may be due to a superposed broad stellar absorption feature of the Hα damped Balmer wing due to the nuclear stellar disk and bulge stars. The nuclear [N II] feature in the PV diagram indicates a steep rise within $\sim 2''$, representing a rapidly rotating nuclear disk. A rigidly rotating PV feature runs across this nuclear PV feature in both the Hα and [N II] lines, which is due to the outer disk component. The rotation curve is flat beyond $R \sim 50''$. Since interstellar extinction by the disk is significant, the nuclear rotation curve may not correctly show up at the present wavelength; the nuclear rise may be much sharper. In fact, the CO line data, which do not suffer from extinction, show a high velocity in the central 5 kpc, where the rotation velocity remains at almost around 250 km s^{-1} (Sofue 1997).

NGC 4569: The [N II] line is stronger than Hα in the nuclear PV component, which shows a steep rise of rotation within $\sim 1''$, though the details are not resolved in the present data. The rotation velocity then attains a minimum at $\sim 15''$, and increases to a flat part beyond $R \sim 30''$.

NGC 4605: No nuclear component is visible. The rotation appears to increase in a rigid-body fashion.

NGC 5033: The nuclear component is superposed by a broad Hα emission feature from the unresolved nucleus, as wide as ~ 1000 km s^{-1}. The [N II] line does not suffer from this nuclear emission, and thus better trace the kinematics. The [N II] PV diagram shows a steep rise of rotation within $\sim 2''$, and then a minimu at $10''$, followed by flat rotation at $R > 15''$.

NGC 5907: This is an almost perfect edge-on Sc galaxy. The nuclear component is not visible because of extinction due to the foreground disk. The disk component shows a rigidly rotating PV feature at $R < 60''$, beyond which the rotation is flat. This rigid-body-like behavior occurs, because we are looking at a ring in the disk, where the optical depth along the lines of sight becomes nearly equal to unity. The CO line data show a sharply rising rotation curve (Sofue 1997).

NGC 7331: The nuclear component is hardly visible in the Hα line, while it is evident in [N II], showing a rapidly rising rotation at $R < 2''$. The rotation of the nuclear disk is rather slow, ~ 100 km s^{-1}. The disk part is clearly traced in the Hα line, reaching a maximum at $R \sim 35''$, beyond which the rotation is flat.

6. Discussion

6.1. Hα vs [N II] Lines

In usual H II regions, the Hα-to-[N II] line intensity ratio (HNR) is almost constant, and both the lines have similar profiles. However, the Hα line profiles in the nuclear regions of some galaxies (e.g., NGC 3521) were found to be superposed by a broad stellar absorption line due to the Balmer wing, most likely by A type stars. In figure 5, we compare the Hα and [N II] lines of NGC 3521 in a gray scale, in order to demonstrate how the Hα Balmer wing affects the PV diagram of the nuclear region. In principle, this will happen to any galaxies if their nuclear region contains a considerable number of A type stars, such as that due to starbursts. Therefore, in this paper we have used the [N II] line for the central regions in place of the Hα line.

The forbidden [N II] line has some advantages for discussing the kinematics of the nuclear regions: it is not affected by the stellar absorption feature, and no particular correction for the difference in wavelength is necessary when used in place of Hα, since both the lines suffer from an almost equal amount of interstellar extinction. The origin of the [N II] line emission is still unclear; it either comes from diffuse regions around the normal H II regions, or from circum-nuclear ionized gas. In either case, its PV behavior would indicate the rotation of the nuclear gas disk, in so far as the [N II]-emitting gas is gravitationally bound to the galaxy. In fact, this will be the case, because the sound velocity of [N II]-emitting gas is on the order of ~ 30 km s^{-1}, or at a temperature $\sim 10^5$ K, and thus the gas cannot escape from the galactic center.

6.2. Comparison with CO-line and Previous Hα Data

Some of the galaxies observed in this paper have been discussed in our recent paper on the CO-line rotation curves (Sofue 1996, 1997). In most cases, the Hα/[N II] rotation curves are consistent with the CO-line rotation curves. This is a natural consequence of the fact that the molecular clouds (CO) and H II regions (Hα-emitting regions) are tightly associated with each other if the optical extinction and absorption are not significant. However, in such galaxies like NGC 3521, whose Hα line is strongly affected by the stellar Balmar absorption wing, the Hα results are not necessarily coincident with the CO results. In such galaxies, the [N II] rotation curves

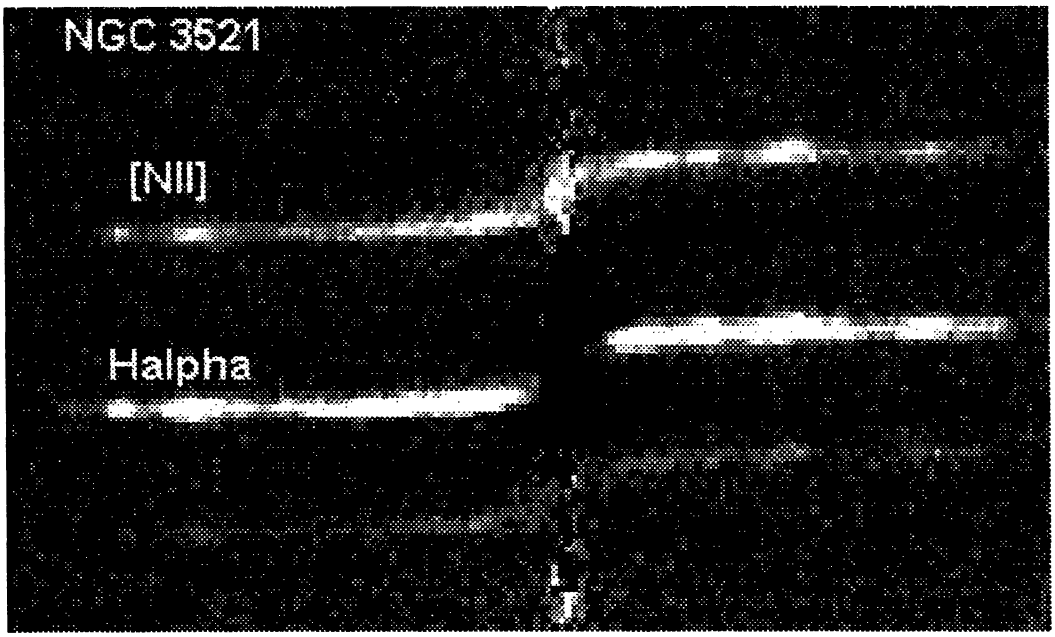

Fig. 5. Hα and [N II] lines of NGC 3521 in a gray scale. This figure demonstrates how the Hα Balmer absorption wing affects the PV diagram of the nuclear region. In such a case, the [N II] line is safer to be used for a rotation curve analysis.

are more consistent with the CO data, which is indeed found to be the case for NGC 3521 (Sofue 1997). Therefore, the [N II] line would be a better tracer of kinematics than the Hα-line for the central regions of galaxies.

The present results are consistent with the recent Hα study of rotation curves of Virgo galaxies by Rubin et al. (1997), who have shown that many galaxies have steeply rising rotation in the center, indicating rapidly rotating nuclear gas disks. However, the nuclear rotation curves derived from our CCD data are not necessarily consistent with the earlier Hα observations using photographic plates (Rubin et al. 1982; Mathewson et al. 1992; Persic et al. 1996), which usually showed a rigid-body increase in the rotation velocity within a few kpc region. This is because of the difference in the dynamic range of observations, particularly in the central regions, where the bright bulge continuum affect the PV diagrams significantly. The earlier photographic data were often saturated in the central bulge regions; also the interest of researchers was more often in the outer flat part of rotation curves, not in the inner details.

6.3. *Steep Nuclear Rise of Rotation and Implication on the Inner Dynamics*

In our earlier paper (Sofue 1996, 1997) we showed that steeply rising rotation curves are common to almost all spiral galaxies of types Sb and Sc, including SBb and SBc, for which high-resolution CO data are available. Such steeply-rising CO rotation in the central region has also been suggested for many southern galaxies (Bajaja et al. 1995), and has been found in many Virgo spirals by the recent Hα spectroscopy (Rubin et al. 1997). This also applies to the present study, and our CCD Hα observations confirm these results. This fact indicates that the mass distribution in the central few hundred parsecs is more steeply increasing toward the nucleus than expected for an exponential-law surface-mass distribution.

By definition, a rotation curve is a trace of terminal velocities in the position–velocity diagram along the major axis. The assumption of axisymmetry and circular rotation has been extensively adopted in deriving the mass of galaxies, including hypothetical dark halos. The thus-derived mass and potential have been widely used to discuss the dynamics of galactic disks, such as the resonance and density waves. In many studies, however, the rotation curve for the central few kpc has been assumed to be rigid-body like.

Resonance: If we adopt such steeply rising rotation curves in place of the widely assumed rigid rotation, dynamical as well as magnetohydrodynamical analyses of the central few kpc region would be significantly affected. Since the epicyclic frequency, $\kappa = \sqrt{1/2}\,\omega\sqrt{1 - d\ln V(R)/d\ln R}$, has a minimum in a rigidly rotating disk, no resonance with the orbital rotation occurs where $\omega = V/R$ is the rotation frequency. The resonance occurs at a radius, where the rotation curve turns from rigid to flat, and the interestellar gas tends to be accumulated so as to make a ring of this

turn-over radius. On the other hand, if the rotation curve is not rigid, but rather flat or even declining, as is often found in sharply peaking rotation curves, this resonance ring occurs at a much smaller radius. Hence, the often-quoted inner rings of radii a few hundred pc to a kpc may not occur in such galaxies having sharply rising rotation curves. In fact, many galaxies appear to not necessarily have a ring structure within the central 1 kpc region; we can trace the outer spiral patterns continuously toward the very nuclear region (e.g., Sofue 1993).

Dynamo: If we adopt the steeply-rising rotation curves, some results concerning the galactic magnetic fields (e.g., Sofue et al. 1986) based on the dynamo theory would be significantly changed for the central regions. The dynamo action depends on the shearing motion of gas from one radius to another. If the rotation is rigid, the shearing motion is minimized, so that the dynamo does not work, resulting in a weak or no magnetic fields in the inner few kpc region. If the rotation is steeply rising and then flat or declining, the shearing motion is more significant and the dynamo action will be more effective, resulting in strong magnetic fields within the inner kpc region.

6.4. *Influence of Bars*

If a galaxy contains a bar, it is not straightforward to derive the mass distribution using the rotation curves. Since dense molecular gas clouds and H II regions are associated with shock-compressed gas lanes along the bar, where the orbital velocity of gas is lowest, their staying probability is highest along the shocked gas lane. On the other hand, the probability is lowest when the gas clouds orbit in the inter-bar regions, where the velocity is highest and nearly parallel to the bar. Therefore, the observed gas clouds and H II regions are most likely observed to exist in the shocked gas lane, which is rotating nearly at the pattern speed of the bar. This means that the apparent rotation velocities may be underestimated compared to the circular velocity, if the galaxy has a bar. Therefore, the presently discussed galaxies would still have a steeper nuclear rise of rotation if they have bars. An analysis of the rotation curves taking into account the effect of a bar is, however, beyond the scope of the present study; the data are still too crude to discuss the bar, for which we need to determine such a large number of parameters, like the mass of the bar, its three axes lengths, orientation of the bar axes with respect to the line of sight, and the shocked gas motion. Therefore, we stress that the present analysis of rotation curves on the assumption of an axi-symmetry can give only a first-order approximation of the mass distribution, which is possibly still underestimated.

6.5. *Slowly-Rising Rotation*

Dwarf and small-mass galaxies: We have seen that a large number of galaxies have a steeply rising rotation curve in the central few kpc region. These steep rises are seen in both Hα and in N II, as long as Hα is not significantly absorbed, as well as in CO. However, there are some exceptions which show rather slowly rising rotation curves in CO, such as in the case of M33 (Sofue 1997). In the present sample, NGC 1003, NGC 2403, and NGC 4605 have such rotation curves in Hα in the central regions. As for NGC 2403, the CO rotation curve also shows a gentle slope in the central 5 kpc region. Therefore, not every galaxy shows a nuclear steep rise.

From figures 3 and 4, one can see that galaxies with gentle rises have smaller disk-rotation velocity than those with a steep nuclear rise. In fact, the maximum rotation velocity of NGC 2403 is about 130 km s^{-1}, and that of NGC 4605 is about 100 km s^{-1}, although it appears to be slightly rising at the observed outermost point. On the other hand, galaxies with steep nuclear rise are likely to have a maximum rotation velocity of $\sim$ 200 km s^{-1} or larger. Also, it is remarkable that those galaxies with a gentle rise do not have prominent bulges, and are classified as Sc or later. Therefore, the slope of nuclear rotation curves are probably correlated with the galaxies' type and mass to some degree. These facts may indicate that less massive galaxies like dwarfs, which have neither a prominent bulge nor a massive core, are likely to show slowly-rising rotation in the nuclear regions, whereas bright galaxies with a disk rotation velocity of $\sim$ 150 km s^{-1} or larger have steeply rising rotation curves, representing their massive bulge and cores.

Edge-on Galaxies: The central regions of edge-on galaxies are obscured by the foreground dust in the disk: the observed rotation curves manifest the rotation of a ring region at which the optical depth through the line of sight becomes about unity. In these cases, although the central steep rise of rotation may not be observed, the derived curves show an apparently rigid rotation. Examples are seen for NGC 3495 and NGC 5907. NGC 4565 is also an edge-on galaxy, while showing a central rise and peak, which may be significantly underestimated. In fact, CO line observations, which do not suffer from interstellar absorption, show a much steeper rise for these edge-on galaxies (Sofue 1997).

The observations were made at the Okayama Astrophysical Observatory of the National Astronomical Observatories. We thank the staff of OAO for their help during the observations.

Reference

Bajaja E., Wielebinski R., Reuter H.-P., Harnet J.I., Hummel E. 1995, A&AS 114, 147

Bosma A. 1981, AJ 86, 1825
Clemens D.P. 1985, ApJ 295, 422
Dressler A., Gunn J.E. 1983, ApJ 270, 7
Honma M., Sofue Y. 1997, PASJ 49, 53
Kent S.M. 1986, AJ 91, 1301
Kent S.M. 1987, AJ 93, 816
Mathewson D.S., Ford V.L. 1996, ApJS 107, 97
Mathewson D.S., Ford V.L., Buchhorn M. 1992, ApJS 81, 413
Osterbrock D.E. 1989, Astrophysics of Gaseous Nebulae and Active Galactic Nuclei (University Science Books, Mill Valley, California)
Persic M., Salucci P. 1995, ApJS 99, 501
Persic M., Salucci P., Stel F. 1996, MNRAS 281, 27
Pierce M.J., Tully R.B. 1992, ApJ 387, 47
Rubin V.C., Ford W.K., Thonnard N. 1980, ApJ 238, 471
Rubin V.C., Ford W.K., Thonnard N., Burstein D. 1982, ApJ 261, 439
Rubin V.C., Kenney J.D.P., Young J.S. 1997, AJ 113, 4
Sofue Y. 1993, PASJ 105, 308
Sofue Y. 1996, ApJ 458, 120
Sofue Y. 1997, PASJ 49, 17
Sofue Y., Fujimoto M., Wielebinski R. 1986, ARA&A 24, 459
Sofue Y., Reich W. 1979, A&AS 38, 251
Sofue Y., Tomita A., Honma M., Tutui Y. 1998, PASJ submitted
Sofue Y., Tutui Y., Honma M., Tomita A. 1997, AJ 114, 2428